JCB Journal of Cell Biology

TOOLS

Quantitative correlative microscopy reveals the ultrastructural distribution of endogenous endosomal proteins

Jan van der Beek, Cecilia de Heus, Nalan Liv, and Judith Klumperman

The key endosomal regulators Rab5, EEA1, and APPL1 are frequently applied in fluorescence microscopy to mark early endosomes, whereas Rab7 is used as a marker for late endosomes and lysosomes. However, endogenous levels of these proteins localize poorly in immuno-EM, and systematic studies on their native ultrastructural distributions are lacking. To address this gap, we here present a quantitative, on-section correlative light and electron microscopy (CLEM) approach. Using the sensitivity of fluorescence microscopy, we label hundreds of organelles that are subsequently visualized by EM and classified by ultrastructure. We show that Rab5 predominantly marks small, endocytic vesicles and early endosomes. EEA1 colocalizes with Rab5 on early endosomes, but unexpectedly also labels Rab5-negative late endosomes, which are positive for PI(3)P but lack Rab7. APPL1 is restricted to small Rab5-positive, tubulo-vesicular profiles. Rab7 primarily labels late endosomes and lysosomes. These data increase our understanding of the structural–functional organization of the endosomal system and introduce quantitative CLEM as a sensitive alternative for immuno-EM.

Introduction

A ubiquitous feature of eukaryotic cells is the division of labor over distinct functional compartments. The endolysosomal system contains different organelles, which together define the ultimate fate of internalized and internal molecules. Mutations in endolysosomal proteins cause severe storage disorders (Marques and Saftig, 2019), and disorganization of the endo-lysosomal system is an underlying cause in cancer, neurological conditions, and many other diseases (Ferguson, 2019; Karabiyik et al., 2017; Lie and Nixon, 2019; Hämälistö and Jäättelä, 2016; Platt et al., 2018). Understanding changes in the endolysosomal system in relation to cellular physiology is therefore a topic of intense research and a fundamental step in elucidating human pathologies.

Endolysosomal compartments are functionally distinguished by their capacity for cargo sorting, recycling, and degradation and, more recently, transcriptional signaling to the nucleus (Ballabio and Bonifacino, 2020). Following internalization from the plasma membrane by small, endocytic tubulo-vesicles, early endosomes uncouple ligands from receptors and sort proteins for recycling or degradation (Huotari and Helenius, 2011; Geuze et al., 1983; Cullen and Steinberg, 2018). Early endosomes mature into late endosomes (Stoorvogel et al., 1991; Poteryaev et al., 2010; Rink et al., 2005), which recycle proteins to the TGN (Rojas et al., 2008; Cullen and Steinberg, 2018) and are capable of fusion with autophagosomes and lysosomes (Bright et al., 2016; Luzio et al., 2010). Late endosome–lysosome fusion generates hybrid endolysosomes, in which active lysosomal hydrolases break down the enclosed material, resulting in lysosomes with an amorphous, dense content. After fusion, membranes are retrieved from the hybrid organelles to form new lysosomes, a process referred to as endocytic lysosome reformation, or autophagic lysosome reformation if fusion with autophagosomes occurred (Yang and Wang, 2021). Degradation by lysosomal hydrolases provides nutrients and new building blocks to the cell. Late endosomes and lysosomes sense the overall nutrient status and signal this to the nucleus to regulate the transcription of lysosome- and autophagy-related genes (Ballabio and Bonifacino, 2020). Together, this highly interconnected and dynamic system of organelles determines protein turnover and maintains cellular homeostasis.

The different endolysosomal compartments are defined by stage-specific molecular machinery and morphologic characteristics (van Meel and Klumperman, 2008; Klumperman and Raposo, 2014; Reggiori and Klumperman, 2016). Small GTPases

Section Cell Biology, Center for Molecular Medicine, University Medical Center Utrecht, Institute of Biomembranes, Utrecht University, Utrecht, the Netherlands.

Correspondence to Judith Klumperman: j.klumperman@umcutrecht.nl.

are the master regulators of membrane trafficking and, together with their effector proteins, mediate fusion, fission, trafficking, and signaling (Pfeffer, 2017; Langemeyer et al., 2018; Puertollano and Bonifacino, 2004; Murray et al., 2016; Schwartz et al., 2017; Ishida and Bonifacino, 2019; D'Agostino et al., 2017; Song et al., 2020; Ohya et al., 2009; Stroupe et al., 2009; Cullen and Steinberg, 2018; Ballabio and Bonifacino, 2020). The small GTPase Rab5 is recruited to newly formed endocytic vesicles and early endosomes (Lee et al., 2006; Mattera et al., 2006; Langemeyer et al., 2018), marking the early stages of endocytosis committed to recycling and sorting. Rab5-positive membranes form two subpopulations by attracting different effector proteins: APPL1 (adaptor protein, phosphotyrosine interacting with PH domain and leucine zipper 1) and EEA1 (early endosome antigen 1; Kalaidzidis et al., 2015; Miaczynska et al., 2004). APPL1 is a multifunctional adaptor protein forming a scaffold for a variety of signaling proteins (Diggins and Webb, 2017) and marks endosomes with a high propensity for fast recycling (Kalaidzidis et al., 2015). The long coiled-coil tether EEA1 enacts fusion between Rab5-positive endocytic vesicles and early endosomal vacuoles as well as homotypic fusion between early endosomes (Murray et al., 2016). Early endosomes also accumulate the regulatory phospholipid phosphatidylinositol 3-phosphate (PI(3)P). EEA1 binds Rab5 and PI(3)P via its opposite ends and remains present on maturing early endosomes (Vanlandingham and Ceresa, 2009) until a change from Rab5 to Rab7 occurs (Rink et al., 2005) that is driven by the Ccz1-Mon1 complex (Poteryaev et al., 2010; Huotari and Helenius, 2011). Rab7 activates numerous effector proteins, including retromer for retrograde trafficking (Liu et al., 2012; Rojas et al., 2008) and the HOPS (homotypic fusion and vacuole protein sorting) tethering complex (Jongsma et al., 2020; van der Beek et al., 2019) required for late endosome–lysosome fusion.

The morphology of endosomes and lysosomes has been studied for many decades using different types of EM methods. These studies have revealed essential structure–function relationships at the nanometer scale (Klumperman and Raposo, 2014). In general, tubules and clathrin coats are associated with sorting and recycling of cargoes (Mari et al., 2008; Sachse et al., 2002b; Willingham et al., 1984; Peden et al., 2004; Raiborg et al., 2006; Geuze et al., 1983), while intraluminal vesicles (ILVs) and dense content are linked to the degradative pathway (Raiborg et al., 2003; Futter et al., 1996; Murk et al., 2003a). In addition, EM has revealed essential information on cellular context, such as type and number of contact sites of endolysosomes with ER and mitochondria (Rocha et al., 2009; Hoffmann et al., 2019; Friedman et al., 2011; Bernhard and Rouiller, 1956; Fermie et al., 2018). Furthermore, immuno-EM methods have been instrumental in localizing proteins to distinct endosomal subdomains, such as recycling tubules, clathrin coats, or ILVs (Mohrmann et al., 2002; Junutula et al., 2004; Fevrier et al., 2004; Biazik et al., 2015; Sönnichsen et al., 2000; Raiborg et al., 2001; Peden et al., 2004; Mari et al., 2008; Sachse et al., 2002b). Collectively, these EM studies have provided an integrated view on the function, molecular composition, and morphology of the different endolysosomal compartments and their subdomains (Klumperman and Raposo, 2014).

Because of their central roles in the endolysosomal system, Rab5, Rab7, EEA1, and APPL1 are the topic of numerous studies. Additionally, Rab5 and EEA1 are frequently used in fluorescence microscopy to mark early endosomes, whereas Rab7 is a commonly used marker for late endosomes and lysosomes (Rink et al., 2005; Kalaidzidis et al., 2015). However, the ultrastructural localization of these proteins has proven difficult, and only few studies have been reported. Using immuno-EM on thawed cryosections, endogenous EEA1 (Mu et al., 1995; Wilson et al., 2000) has been localized to early endosomal vacuoles and overexpressed Rab7-GFP to late endosomes, lysosomes, and autophagosomes (Bucci et al., 2000; Jäger et al., 2004). APPL1 has been detected on tubular endosomes using preembedding labeling and silver enhancement (Kalaidzidis et al., 2015), as well as through immuno-EM using a noncommercial antibody (Miaczynska et al., 2004). Using superresolution correlative light and electron microscopy (CLEM) on 250-nm cryosections, Franke et al. (2019) localized Rab5-GFP to restricted domains of early endosomal vacuoles. However, none of these approaches included a systematic, quantitative analysis of the ultrastructural distribution of these proteins. Nor has simultaneous labeling of multiple markers been performed. Moreover, the use of overexpression approaches may induce artifacts in endolysosomal morphology and lead to nonspecific membrane associations (Bucci et al., 2000). Thus, a robust, quantitative ultrastructural analysis of organelles that are Rab5-, Rab7-, EEA1-, or APPL1-positive is currently lacking. Additionally, it remains unknown how their distribution relates to the commonly used morphologic definitions of endolysosomal organelles used in EM studies.

To connect functional-molecular information to morphology, we here present a quantitative CLEM approach based on the use of ultrathin cryosections. Using optimized strategies for correlation, we detect the endosomal marker proteins by fluorescence microscopy and then image the same sample in EM for accurate correlation of fluorescence labeling to ultrastructure (Mohammadian et al., 2019; Cortese et al., 2012; Vicidomini et al., 2008). This enables the correlation of hundreds of fluorescent spots to endolysosomal morphology, followed by a systematic categorization based on ultrastructure. Our data highlight the distinction between endocytic tubulo-vesicles, APPL1 endosomes, and early endosomes and show that the widely used marker for early endosomes, EEA1, in fact is an appropriate marker for both early and late endosomes. This approach introduces CLEM as a sensitive and quantitative protein localization method that is a feasible and attractive addition to classic immuno-EM methods.

Results

Immunofluorescence (IF) of endogenous Rab5, Rab7, APPL1, and EEA1 reveals distinct organelle populations

We selected a panel of commercially available antibodies against Rab5, Rab7, APPL1, and EEA1 that have been widely used in IF studies (Fig. 1; and Table 1) and first tested these in a conventional IF protocol on permeabilized HeLa cells fixed in 4% formaldehyde (FA). With multiple double-labeling combinations,

we addressed the colocalization between the different proteins (Fig. 1).

We found Rab5-positive endosomes distributed over the cell periphery and perinuclear area (Fig. 1, A, D, and E), whereas Rab7-positive compartments were enriched in the perinuclear area (Fig. 1, A–C). Due to the efficiency of Rab5 to Rab7 conversion by the Mon1-Ccz1 complex (Poteryaev et al., 2010), only a few endosomes with both Rab5 and Rab7 were expected. Indeed, only 6% of the Rab5-positive spots were also labeled for Rab7 (Fig. 1 A). Conversely, 24% of the Rab7-positive spots were also positive for Rab5 (Fig. 1 G). The rest of Rab5 or Rab7 spots formed separate pools. Rab5-positive spots partially overlapped with either EEA1 (26%) or APPL1 (45%; Fig. 1, D, E, and I).

Rab7-positive spots showed 35% and 22% overlap with the late endosomal/lysosomal markers CD63 and Cathepsin D, respectively (Barrett, 1980; Pols and Klumperman, 2009; Fig. 1, B, C, and H). Hence, a sizeable portion (57%) of Rab7-positive compartments do not contain CD63 or Cathepsin D, which is somewhat unexpected but has several putative explanations. First, it is feasible that CD63 and Cathepsin D are present on only a subset of endosomes and lysosomes. Second, the spatial segregation between luminal CD63 and Cathepsin D and membrane-associated Rab7 may decrease the level of colocalization (Fig. 1 H). Last, Rab7 in addition to endosomes can also be found on small vesicles, as reported before (Rojas et al., 2008) and seen in Figs. 3 D and S6, C–E.

APPL1 is recruited to membranes through interaction with Rab5 (Diggins and Webb, 2017) and via its BAR domain, which binds to curved membranes (Zhu et al., 2007; Mim and Unger, 2012). EEA1 is recruited to membranes by Rab5 and PI(3)P. In previous live-cell imaging studies of fluorescently tagged proteins (Kalaidzidis et al., 2015), APPL1 and EEA1 were found on distinct pools of endosomes that both receive endocytosed material from the plasma membrane. Cargo present in APPL1 endosomes is either sorted into a fast-recycling pathway to the plasma membrane or transferred to EEA1 endosomes, where further sorting for recycling or degradation occurs. By IF of HeLa cells, we confirmed (Kalaidzidis et al., 2015; Miaczynska et al., 2004) that EEA1 and APPL1 spots show little overlap (Fig. 1, F and I), while both populations colocalize with Rab5 (Fig. 1, D, E, and I). As also reported before, the APPL1 spots were mostly confined to a region just below the plasma membrane (Fig. 1 E, arrows; Kalaidzidis et al., 2015).

These IF experiments show that the selected antibodies label distinct types of endolysosomal subpopulations, of which the majority are positive for Rab5, Rab5/EEA1, Rab5/APPL1, or Rab7, respectively. It is unknown, however, how much these subpopulations coincide with morphologic definitions, since systemic immuno-EM studies of these proteins are lacking.

Immunolabeling of selected antigens on ultrathin sections yields label for IF but not EM

Tokuyasu cryosections are routinely used for immuno-EM (Slot and Geuze, 2007; Möbius and Posthuma, 2019). The use of mild fixatives and the lack of permeabilizing agents and embedding media results in an effective immuno-EM method, while the negative staining procedure gives optimal membrane contrast (Slot and Geuze, 2007; Möbius and Posthuma, 2019). More recently, cryosections were also proven excellent tools for IF and on-section CLEM, since they yield a high fluorescent signal-to-noise ratio (SNR; Oorschot et al., 2014; Mohammadian et al., 2019; Cortese et al., 2012; Vicidomini et al., 2008). To test the performance of the selected antibodies (Table 1) on cryosections, we fixed HeLa cells with 4% FA for 1 h and processed them into either 250-nm semithick cryosections for on-section IF or 90-nm ultrathin cryosections for immunogold labeling and transmission EM (TEM; see Materials and methods; Möbius and Posthuma, 2019; Slot and Geuze, 2007). Before fixation, we had incubated cells for 3 h with the endocytic marker BSA coupled to 5-nm gold particles (BSA^5), which is visible by EM. Sections were incubated with the selected primary antibodies, followed by Alexa Fluor–conjugated antibodies for IF or with protein A conjugated to 10- or 15-nm gold particles for immuno-EM, using established protocols (Slot and Geuze, 2007).

We first tested several dilutions of the commercially available Rab5, Rab7, EEA1, and APPL1 antibodies for IF on 250-nm cryosections (not depicted). After establishing the optimal dilutions (Table 1), all antibodies gave a distinct labeling pattern and performed well in on-section colocalization studies (Fig. 2, A–C). However, when using these same antibodies (in dilutions from 1:10 to 1:100) on ultrathin cryosections and using our immuno-EM protocol, we found no significant specific labeling for any of the antigens (Fig. 2, D and E). As a positive control, we double-labeled for Hrs (an ESCRT-0 component marking early endosomes) or CD63 (Pols and Klumperman, 2009; Gao et al., 2019), which yielded specific gold labeling in EM. Since the primary antibodies for Rab5, Rab7, EEA1, and APPL1 are identical in IF and EM, the discrepancy in labeling is likely explained by the use of different reagents, labeling strategies, and postlabeling procedures.

An important implication from these data is that labeling of cryosections—instead of using whole cells as in conventional IF studies—allows for detection of the selected endosomal marker proteins by IF, but not EM. The IF labeling, however, opens the way for on-section CLEM.

An optimal fixation protocol for fluorescence labeling and ultrastructure

In on-section CLEM, a section is first viewed by fluorescence microscopy and then by EM. Recent developments by us (Mohammadian et al., 2019; Fermie et al., 2021 *Preprint*) and others (Paul-Gilloteaux et al., 2017; Mastronarde, 2018; Cortese et al., 2012) have improved the accuracy and correlation efficiency of on-section CLEM to such an extent that the fluorescent signal can be directly inferred to EM sections. Unlike IF, however, preservation of ultrastructure is key for interpretation of EM data. As shown in Figs. 1 and 2, the antibodies for Rab5, Rab7, EEA1, and APPL1 work well in IF of HeLa cells fixed in 4% FA for 15 or 60 min. These short fixation times, however, generally result in poor EM ultrastructure. Stronger fixatives better preserve ultrastructure but often abolish antigenicity. To establish the optimal balance between fluorescent signal and EM ultrastructure, we performed eight different fixation regimes on HeLa cells (Table 2) and processed them into 90-nm

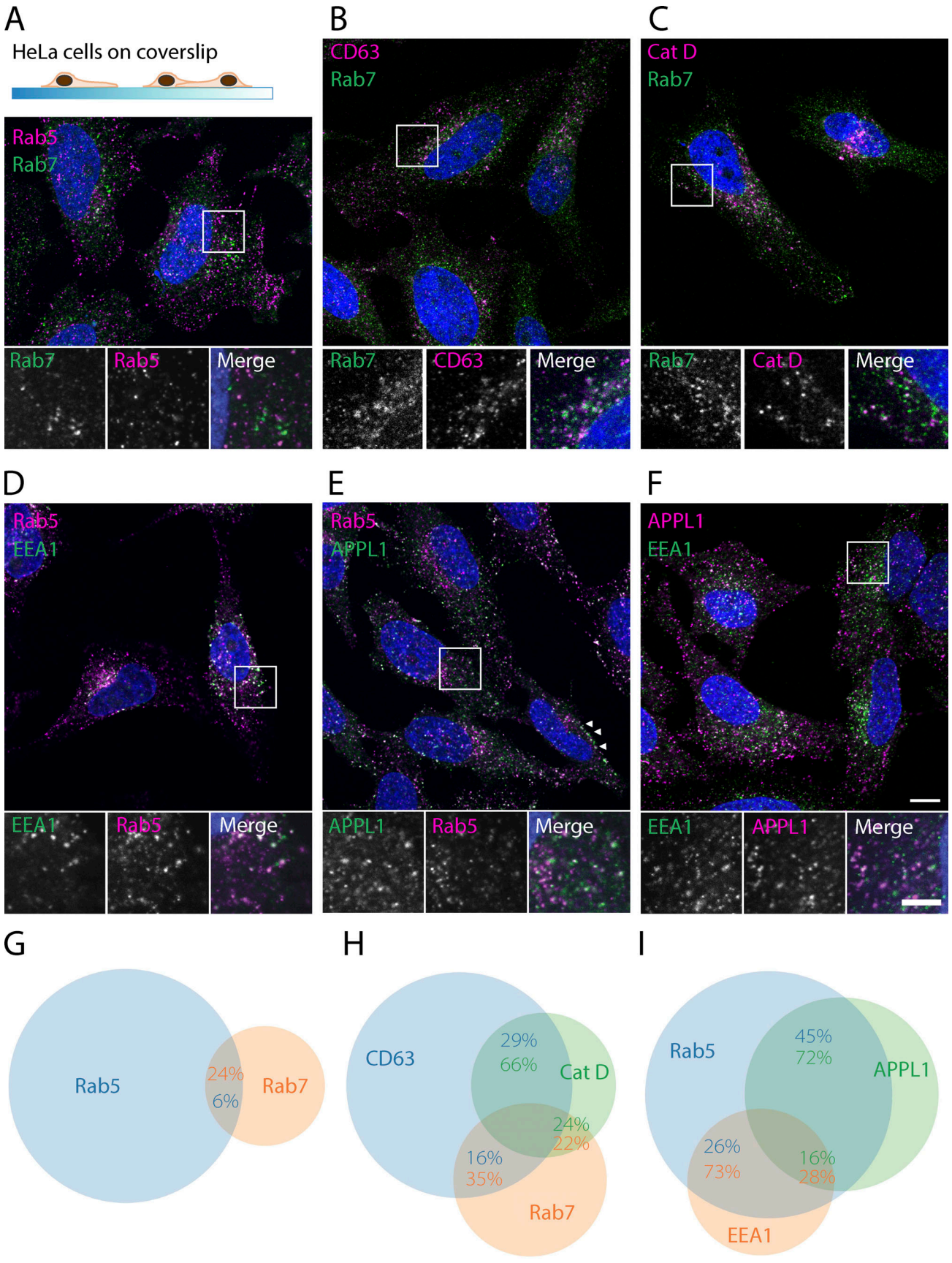

Figure 1. **IF of endolysosomal markers reveals overlapping yet separate localization patterns.** Pictures are confocal images (slices) of double-labeled, permeabilized HeLa cells fixed with 4% FA. **(A)** Rab5 and Rab7 predominantly mark separate organelles. **(B and C)** Rab7 partially colocalizes with CD63 and

Cathepsin D. **(D)** EEA1 labels a perinuclear subpopulation of Rab5 endosomes. **(E)** APPL1 labels a peripheral pool of Rab5 endosomes. Note the presence of APPL1 endosomes just below the plasma membrane (arrowheads). **(F)** EEA1 and APPL1 show little overlap. **(G–I)** Venn diagrams based on colocalization analysis of labeling combinations in A–F. Circle size is proportional to total dots detected for a protein, overlap to number of colocalized dots. Images were analyzed by dot detection in two or three channels, after which overlapping dots were classified as colocalized particles. Percentages represent the colocalized fraction of the correspondingly colored protein. See Materials and methods for a more detailed description of the analysis; see Table S1 for SDs and cell and organelle numbers. Scale bars, 10 µm in larger images; 5 µm in insets.

cryosections that were labeled for IF or contrasted with uranyl acetate (UA) and examined by TEM. To calculate the SNR of the IF labeling, we took the mean intensity value of the 0.5% brightest pixels divided by the mean intensity value of the reverse selection. To classify EM morphology, a panel of laboratory members blindly ranked the EM images on the visibility and sharpness of membranes and overall cohesion of the cytoplasm (Table 2).

We found that 30-min fixation with 4% FA generally yielded the best SNR in IF; however, preservation of EM morphology was very poor in these conditions (Table 2 and Fig. S1). Adding 0.2% glutaraldehyde (GA) greatly improved EM morphology (Table 2 and Fig. S2) but deteriorated the fluorescence signal even when we quenched GA autofluorescence with $NaBH_4$. Using only FA, we found for all antibodies that increased fixation times significantly decreased the IF signal (Table 2), with a steep decline after 1 h. As an optimal compromise between fluorescence signal and morphology, we selected a mild fixation of 4% FA for 1 h as the best fixative for CLEM.

Table 1. **Antibodies used in this study**

Antibody	Company and catalog number	Concentration used	Reference
Mouse anti-EEA1	BD Transduction Lab #610457	1:200 (IF), 1:150 (CLEM)	Ploper et al., 2015
Rabbit anti-APPL1	Cell Signaling Technology #3858	1:200 (IF), 1:150 (CLEM)	Sneeggen et al., 2019
Rabbit anti-EEA1	Cell Signaling Technology #C45B10	1:200 (IF), 1:150 (CLEM)	Ploper et al., 2015
Mouse anti-Rab5	BD Biosciences #610725	1:200 (IF), 1:10 (immuno-EM), 1:150 (CLEM)	Kurgonaite et al., 2015
Mouse anti-CD63	Developmental Studies Hybridoma Bank #H5C6	1:500 (IF), 1:300 (immuno-EM)	Ploper et al., 2015
Rabbit anti-Rab7	Cell Signaling #9367	1:200 (IF), 1:10 (immuno-EM), 1:150 (CLEM)	Marwaha et al., 2017
Goat anti-Cathepsin D	R&D Systems #AF1014	1:500 (IF)	Gao et al., 2019
Rabbit anti-Hrs	Santa Cruz #SC-30221	1:50 (immuno-EM)	Meister et al., 2017
Donkey anti-mouse Alexa Fluor 488	Life Technologies #A21202	1:250 (IF, CLEM)	
Donkey anti-rabbit Alexa Fluor 568	Life Technologies #A10042	1:250 (IF, CLEM)	
Donkey anti-goat Alexa Fluor 647	Life Technologies #A21447	1:250 (IF)	
Goat anti-mouse Alexa Fluor 647	Invitrogen #A28181	1:250 (CLEM)	
Rabbit anti-mouse	Zymed #61-6800	1:500 (immuno-EM)	

CLEM of Rab5 and Rab7 reveals differential distributions over early to late endolysosomal compartments

We then executed a full CLEM experiment by performing IF and EM on the same section (Fig. 3 A; full protocol provided in Materials and methods). In brief, we incubated HeLa cells for 3 h with BSA[5], fixed cells for 1 h in 4% FA, and then immediately scraped cells to prepare ±1 mm^3 gelatin blocks that were plunge-frozen and stored in liquid nitrogen. We collected 90-nm cryosections from these blocks on an EM carrier grid and labeled them with the selected primary antibodies, Alexa Fluor–tagged fluorescent secondary antibodies, and DAPI to stain the nuclei. The fluorescently labeled sections were imaged in a wide-field fluorescence microscope, collecting tilesets of the ribbon of sections on the grid (Mohammadian et al., 2019; Cortese et al., 2012). After imaging, the grids were stained with 2% UA, which is our normal contrasting procedure for immuno-EM. In the EM, we again collected large image tilesets at 43,000× magnification to resolve endolysosomal membranes in great detail and stitched them together using Etomo postprocessing software. The nuclei, in IF identified by DAPI signal and in EM by morphology, served as numerous unique reference points that made the correlation between the IF and EM images highly accurate (Fig. S3). Combining these large datasets of fluorescence microscopy and EM allows correlation of hundreds of organelles from tens of cells in one sample, which greatly increases the throughput of on-section CLEM.

We first applied quantitative CLEM on sections of HeLa cells double-labeled for endogenous Rab5 and Rab7 (Fig. 3). We could readily define Rab5-, Rab7-, and Rab5/7-positive puncta by their fluorescent signal (Fig. 3 B) and correlated them to EM ultrastructure. By EM, we classified the underlying structures as vesicle-tubule, early or late endosome, or lysosome based on morphologic criteria coming from a wealth of previous (immuno-)EM studies from many distinct laboratories (Vogel et al., 2015; Sachse et al., 2002a; Rojas et al., 2008; Mari et al., 2008; for additional references, see reviews: Klumperman and Raposo, 2014; Reggiori and Klumperman, 2016; Gruenberg and Stenmark, 2004; for summary of the criteria, see Materials and methods). Based on these ultrastructural definitions, our on-section CLEM approach localized Rab5 mainly to vesicles and

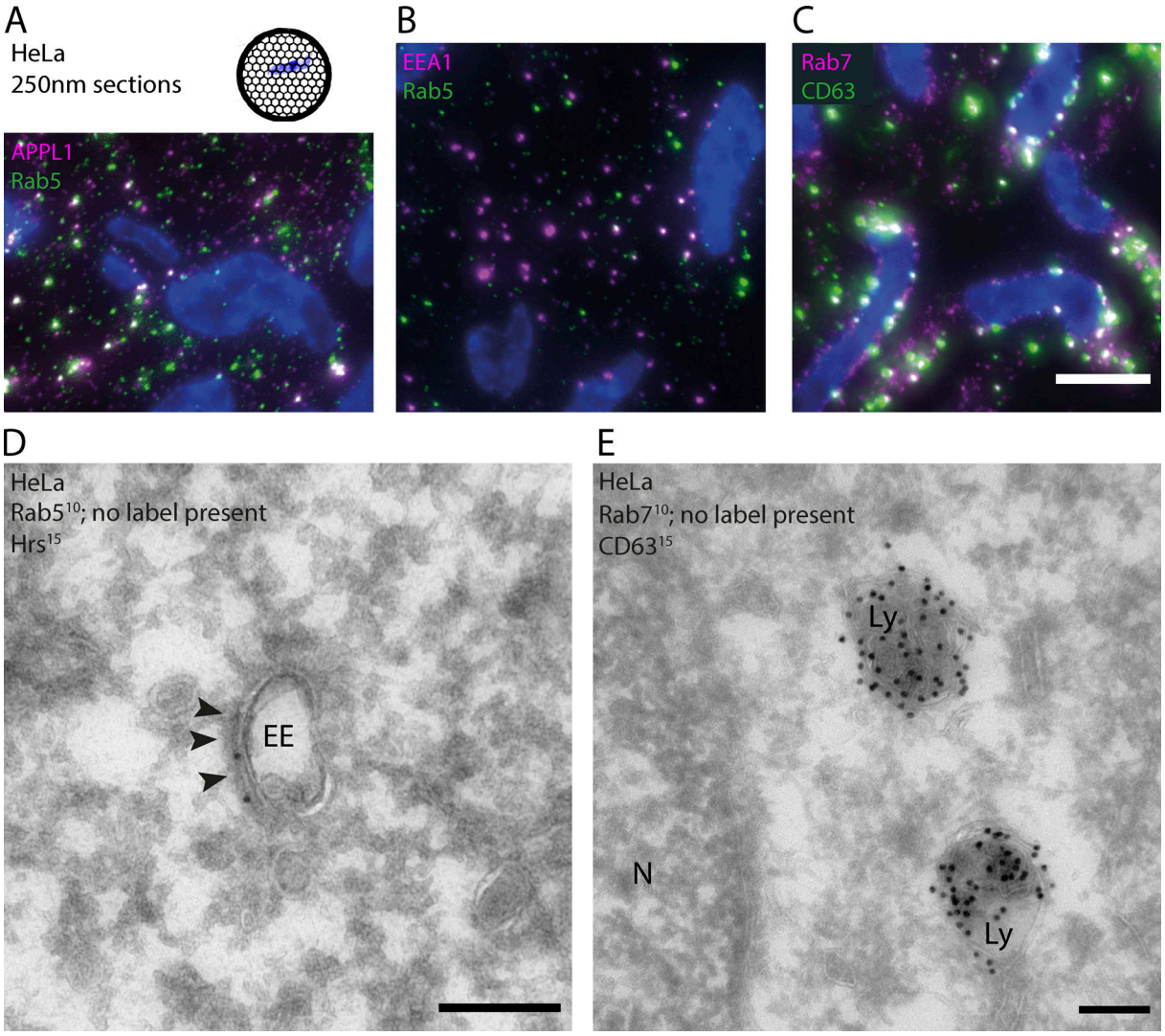

Figure 2. **Immunostaining of Rab5 and Rab7 on cryosections yields fluorescent but no immunogold labeling.** HeLa cells fixed with 4% FA for 1 h and processed into 250-nm cryosections imaged by wide-field microscopy (A–C) or 90-nm cryosections imaged by TEM (D and E). **(A–C)** On-section immunolabeling for Rab5, Rab7, CD63, EEA1, and APPL1 in indicated combinations using the same primary and secondary antibodies as in Fig. 1. Scale bar, 5 µm. **(D and E)** Double-immunogold labeling following our established immuno-EM protocol (Slot and Geuze, 2007) using the same primary antibodies as in A–C and protein-A gold (gold sizes indicated in superscript). Arrowheads indicate clathrin coats. **(D)** Early endosome (EE) labeled for Hrs (15-nm gold) as positive control for the immuno-EM procedure. Rab5 (10-nm gold) cannot be detected by immuno-EM. **(E)** Lysosomes (Ly) abundantly labeled for the late endosomal/lysosomal protein CD63 (15-nm gold) labeling, whereas no Rab7 label (10-nm gold) is detected. N; nucleus. Scale bars, 200 nm.

tubules (70%) and only a relatively minor part to early endosomes (19%). The Rab5-positive vesicle-tubules were 100–200 nm in diameter and often found near the plasma membrane. In agreement with a role in endocytosis, they occasionally contained internalized BSA[5], and 23% of the correlated vesicle-tubules showed a distinctive clathrin coat. Of the Rab5-positive early endosomes, 43% were positive for endocytosed BSA[5] and 57% displayed the characteristic flat, bilayered clathrin coat within the plane of sectioning (Fig. 3 C, arrowheads; see Fig. S4 A for uncolored images). Our results thereby match the existing literature, where Rab5 has been described both on endocytic vesicles (McLauchlan et al., 1998) and on endosomal vacuoles (Franke et al., 2019). We found only 5% of Rab5 staining over compartments that met the morphologic criteria of late endosomes (Fig. 3 D).

Rab7 showed a very different distribution pattern by labeling mostly late endosomes (33%) and lysosomes (39%; Fig. 3 D). 86% of Rab7-positive late endosomes and 44% of Rab7-positive lysosomes contained BSA[5] (3-h uptake), which reflects the kinetics by which these distinct stages of the endocytic pathway are reached. Of note, the presence of BSA[5] cannot be used to measure the total number of organelles reached by endocytic marker, since some negative organelles may contain BSA[5] outside the plane of sectioning, especially when colloidal gold particles become clustered after degradation of BSA. In case quantitative studies on the entire endolysosomal system are required, the use of lysine-fixable fluorescent fluid phase markers, which fill the entire lumen of endocytic organelles, is advised. Only 6% of all analyzed compartments were positive for both Rab5 and Rab7, and the organelles underlying these double-

Table 2. **Effect of fixation on IF intensity and EM morphology**

Fixation Protocol	IF SNR Rab5	IF SNR Rab7	IF SNR EEA1	IF SNR APPL1	EM Morphology	Figure
30-min FA 4%	2.09 ± 0.05	1.61 ± 0.03	2.00 ± 0.06	2.30 ± 0.11	–	Fig. S1 A
1-h FA 4%	1.72 ± 0.15	1.66 ± 0.07	1.76 ± 0.08	1.85 ± 0.06	+/–	Fig. S1 B
2-h FA 4%	1.62 ± 0.34	1.51 ± 0.03	1.42 ± 0.04	1.63 ± 0.03	+/–	Fig. S1 C
1-h FA 4% → ON FA 0.6%	1.44 ± 0.07	1.48 ± 0.06	1.41 ± 0.04	1.66 ± 0.06	+	Fig. S1 D
ON FA 4%	1.43 ± 0.13	1.51 ± 0.02	1.24 ± 0.02	1.31 ± 0.02	+	Fig. S2 A
30-min FA 4% + GA 0.2%	1.66 ± 0.06	1.36 ± 0.03	1.20 ± 0.04	1.28 ± 0.08	++	Fig. S2 B
2-h FA 4% + GA 0.2%	1.70 ± 0.02	1.41 ± 0.03	1.34 ± 0.05	1.39 ± 0.04	++	Fig. S2 C
ON FA 4% + GA 0.2%	1.64 ± 0.04	1.36 ± 0.02	1.25 ± 0.01	1.30 ± 0.02	++	Fig. S2 D

90-nm cryosections of HeLa cells fixed according to the indicated protocols were fluorescently labeled and imaged using fixed settings. The SNR was calculated as mean intensity value of the 0.5% brightest pixels divided by the mean intensity value of the reverse selection. Five fields-of-view were averaged for each measurement. Most SNRs significantly declined upon >30-min FA fixation or addition of GA. Morphological quality of EM images was based on blind ranking by six experienced electron microscopists. Based on these measurements, 1-h fixation with 4% FA was chosen as best fixative for CLEM.

labeled puncta had both early and late endosomal characteristics. Overall, the Rab7 distribution pattern is in line with previous studies (Bucci et al., 2000; Rojas et al., 2008) and supports Rab7's role as an organizer of the late endocytic pathway.

By correlating a large number of organelles (n = 101), we systematically categorized the distribution patterns of Rab5 and Rab7 over the distinct endolysosomal organelles (Fig. 3 D). This showed that endogenous Rab5 is generally distributed over vesicles, tubules, and early endosomes, while Rab7 is found over late endosomes and lysosomes. Interestingly, the majority of Rab5 in HeLa cells is present on small endocytic vesicles rather than on early endosomal vacuoles, which are two functionally distinct stages of the early endocytic pathway.

In general, the distributions correspond to the known functions and localizations of these Rabs. This demonstrates the feasibility of our approach in using the sensitivity of fluorescence microscopy to study ultrastructural distributions of endogenous proteins in a robust, quantitative manner.

CLEM localizes EEA1 and APPL1 to morphologically different compartments

Next, we performed on-section CLEM on HeLa cells double-labeled for APPL1 and EEA1 (Fig. 4). Using the same morphologic definitions as for Rab5 and Rab7, we found that APPL1 and EEA1 have very different localization patterns and seldom overlap (only 5% of all analyzed organelles; Fig. 4, A and D). APPL1 staining consistently marked tubulo-vesicular membranes of 100–150-nm diameter, sometimes clustered together (Fig. 4 B). This is in line with a previous preembedding immunolabeling study (Kalaidzidis et al., 2015) showing APPL1 on vesicular structures rather than classic early endosomes. Following existing literature, we refer to these APPL1 tubulo-vesicles as APPL1 endosomes (Kalaidzidis et al., 2015; Miaczynska et al., 2004). We found APPL1 endosomes often in the vicinity of the plasma membrane, which matches the pattern observed in IF. Analysis of 53 APPL1 endosomes showed that 30% exhibited a clathrin coat (Fig. 4 D, arrows) and 25% contained internalized BSA[5], consistent with their endocytic nature. Since accumulation of APPL1 on endosomes coincides with loss of clathrin (Zoncu et al., 2009), APPL1 endosomes with a clathrin coat are likely freshly derived from the plasma membrane, while those without are older. Notably, APPL1 endosomes lacked any other morphologic characteristics; they formed no membrane buds or branches and displayed no internal membranes. By contrast, EEA1 was found on a variety of endosomal organelles, ranging from small (100–200 nm) endocytic vesicles to classic early endosomes with ILVs and bilayered clathrin coats (Fig. 4, B and D, arrowheads). Unexpectedly, EEA1 was also found on typical late endosomes and even lysosomes (Fig. 4 B). Quantification showed that about half of the fluorescent EEA1 puncta localized to these late endolysosomal compartments (Fig. 4 C). In the case of EEA1 and APPL1 colocalization by IF, this often revealed an early endosome with a vesicle in close vicinity, thus representing separate EEA1- and APPL1-labeled compartments (Fig. 4 D).

EEA1 localizes to late endosomal compartments that lack Rab5

EEA1 is generally considered an early endosomal protein, since it binds Rab5 (Mishra et al., 2010) and interacts through its FYVE domain with PI(3)P (Gaullier et al., 1998; Stenmark et al., 1996), which is enriched on early endosomes (Gillooly et al., 2003). The relatively high percentage of EEA1 on late endosomal compartments (Fig. 4 C) was therefore unexpected, especially since Rab5 was rarely seen on late endosomes (only 5% of all Rab5 positive compartments; Fig. 3 D) and virtually absent from lysosomes. Since IF showed that 27% of the EEA1 puncta were negative for Rab5 (Fig. 1, D, E, and I), these data suggest that part of EEA1 is present on Rab5-negative late endosomal compartments. To address this, we performed CLEM double-labeling for EEA1 and Rab5 (Fig. 5 A; see Fig. S5 for uncolored images) and quantitated their colocalization behavior per category of endosomal organelle: 100–200-nm vesicle-tubules, early endosomes, and late endosomes (Fig. 5 B). Of all fluorescently labeled 100–200-nm vesicle-tubules, the majority (52%) displayed only Rab5 (part of these will be APPL1 endosomes), 27% both Rab5 and EEA1, and

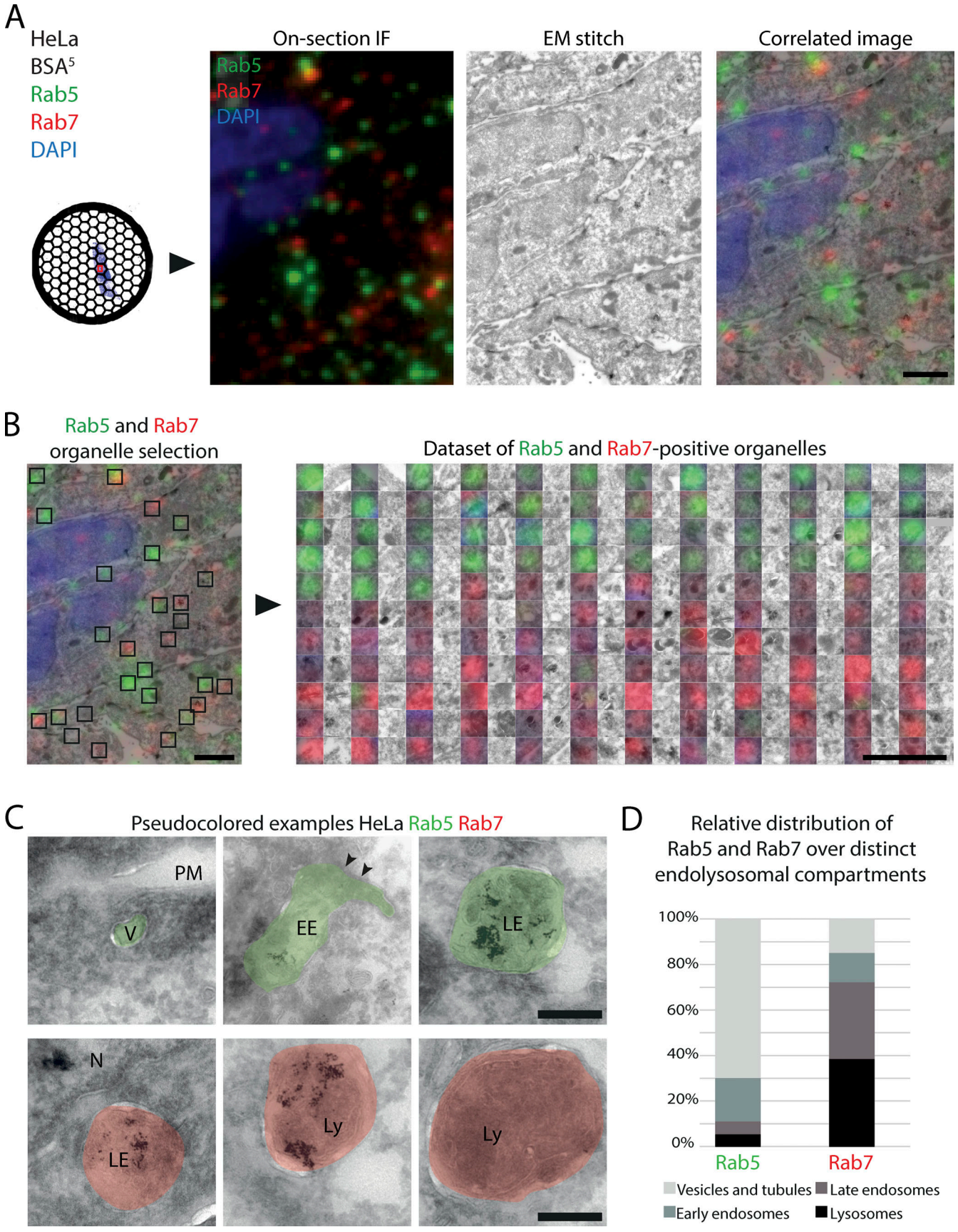

Figure 3. **On-section CLEM of Rab5 and Rab7 reveals complementary distributions over early and late endolysosomal compartments.** CLEM of Hela cells fixed with 4% FA for 1 h. Before fixation, cells were incubated with BSA[5] for 3 h. **(A)** Left: Wide-field image of part of a 90-nm cryosection labeled for Rab5

and Rab7 and Alexa Fluor 488 and 568 secondary antibodies, respectively. Middle: Stitched EM image of the same area composed of 63 43,000× magnification images. Right: Overlay of IF and EM images. **(B)** Left: Low-magnification overview of organelles selected for correlation (indicated by black squares). Right: Dataset of IF- to EM-correlated Rab5- and Rab7-positive organelles. Each left row shows the CLEM overlay with the EM-only image at right. **(C)** Zoom-ins of pseudocolored examples of organelles positive for Rab5 (green) and Rab7 (red). Some organelles contain internalized BSA[5]. Arrowheads indicate clathrin coats. For uncolored images, see Fig. S4 A. **(D)** Relative distribution of Rab5 and Rab7 over distinct endolysosomal compartments as identified by morphology. Rab5 prevails on endocytic vesicles-tubules and early endosomes, and Rab7 on late endosomes and lysosomes. *n* = 37 for Rab5 and 64 for Rab7, taken from three double-labeled samples. EE, early endosome; LE, late endosome; Ly, lysosome; N, nucleus; PM, plasma membrane; V, vesicle. Scale bars, 2 µm in A and B; 200 nm in C.

21% only EEA1 (Fig. 5 B). Of the classic early endosomes, i.e., with a distinctive vacuolar part and containing ILVs, about half (44%) contained both Rab5 and EEA1 and the other half (51%) only EEA1. The vast majority (77%) of labeled late endosomes contained only EEA1, while 18% were positive for both Rab5 and EEA1. Only 5% of all labeled endosomes were positive for Rab5 alone.

These data clearly show that Rab5 and EEA1 have distinct distributions: Rab5 is mostly confined to early-stage endocytic vesicles and early endosomes, whereas EEA1, in addition to early endosomes, labels late endosomal compartments, the majority of which lack Rab5. The highest degree in colocalization between Rab5 and EEA1 occurs on early endosomes.

EEA1 localizes with PI(3)P on late endosomes

The presence of EEA1 on late endosomes that lack Rab5 raised the question of how EEA1 is anchored to these membranes. EEA1, in addition to its Rab5-binding domain, has a PI(3)P-binding FYVE domain. To test whether PI(3)P could localize EEA1 to late endosomes, we prepared HeLa cells expressing a construct of two Hrs-derived FYVE domains fused to GFP, a PI(3)P-specific probe (Gillooly et al., 2003) that is widely used in studies of the endolysosomal system. The 2xFYVE-EGFP probe yielded a clear signal in ultrathin cryosections, demonstrating another advantage of this method, i.e., that the GFP signal remains visible (Fig. S6 A). We then combined the in-section GFP signal with on-section double-immunolabeling of Rab5 and EEA1 for quantitative CLEM. Since high expression levels of the 2xFYVE-EGFP probe induced enlargement and clustering of endosomes, we included only low-expressing cells in these analyses (Fig. S6 A, outlined cells). By CLEM, we found that 38% of the PI(3)P label associated with early endosomes, and another significant portion (50%) with late endosomes, most of which were also positive for Rab5, EEA1, or both (Fig. 5 C). Colocalization analysis showed that most (65%) PI(3)P/Rab5/EEA1-positive puncta were early endosomes, whereas 29% represented late endosomes (Fig. 5 D). By contrast, most PI(3)P/EEA1-positive, Rab5-negative puncta identified as late endosome (52%) or lysosome (9%).

These data show a trend in which early endosomes contain Rab5, EEA1, and PI(3)P, while late endosomes lack Rab5 but still display EEA1 and PI(3)P (see Fig. 7 for a schematic representation). This implies that after Rab5 dissociation from early endosomes, EEA1 remains on late endosomes through its interaction with PI(3)P (Lawe et al., 2002).

EEA1-positive late endosomes are negative for Rab7

Since the dissociation of Rab5 coincides with the recruitment of Rab7 (Rink et al., 2005; Poteryaev et al., 2010), we next investigated if the EEA1-positive/Rab5-negative late endosomes (Fig. 5, A and B) contain Rab7. Strikingly, IF of double-labeled, 90-nm ultrathin cryosections of HeLa cells revealed minimal Rab7 and EEA1 colocalization; <5% of the EEA1 spots overlapped with Rab7 (Fig. 5, E and F), which is in accordance with previously reported IF on whole cells (Vonderheit and Helenius, 2005). By CLEM, we could readily identify EEA1-positive late endosomes that were negative for Rab7 (Fig. 5 G). Moreover, part of the few EEA1/Rab7 spots appeared to be false positives, i.e., fluorescence caused by a fold in the section or a dirt particle (Fig. 5 E, solid arrowhead; and Fig. S6 B). Some adjacent EEA1 and Rab7 fluorescent spots (Fig. 5 E, open arrowhead; and Fig. S6 C), were identified by CLEM as EEA1-positive endosomes surrounded by Rab7-positive vesicles (Fig. S6, C–E). The latter might represent Rab7/retromer-positive recycling tubules, emerging from endosomes where EEA1 is still maintained by the lipid PI(3)P (Fig. 5, C and D; Simonsen et al., 1998; Murray et al., 2016; Liu et al., 2017). Combined, our data suggest the existence of a pool of EEA1-positive endosomes that is not substantially labeled by Rab5 or Rab7, but may form Rab7-positive recycling membranes.

EEA1 localization to late endosomes is conserved between cell lines

To investigate whether the unexpected association of EEA1 with late endosomes is representative for the general distribution of EEA1, we next performed on-section CLEM of EEA1 in HepPG2 (human hepatoma), A549 (human adenocarcinoma from alveolar basal epithelium), and HT1080 (human fibrosarcoma) cell lines (Fig. 6, A–C; see Fig. S7 for uncolored images). We combined this with APPL1 staining. In all cell lines, we found substantial EEA1 label on late endosomal compartments, although the relative distributions differed: 45%, 29%, and 15% of total labeling in HepG2, HT1080, and A549 cells, respectively (Fig. 6 D). Notably, in A549 and HT1080 cells, a considerable portion of EEA1 (44% and 41%, respectively) was also found on 100–200-nm vesicles, presumably endocytic vesicles. APPL1 in all cell lines localized to the typical tubulo-vesicular APPL1 endosomes, with limited overlap with EEA1 (Fig. 6 D).

These quantitative data show, across multiple cell lines, that EEA1 has a more widespread distribution toward late endosomal compartments than thus far anticipated. We also show that the relative distribution of endosomal proteins differs between cell lines.

Discussion

In this paper, we introduce a sensitive CLEM method to robustly study the ultrastructural distribution of selected proteins. By

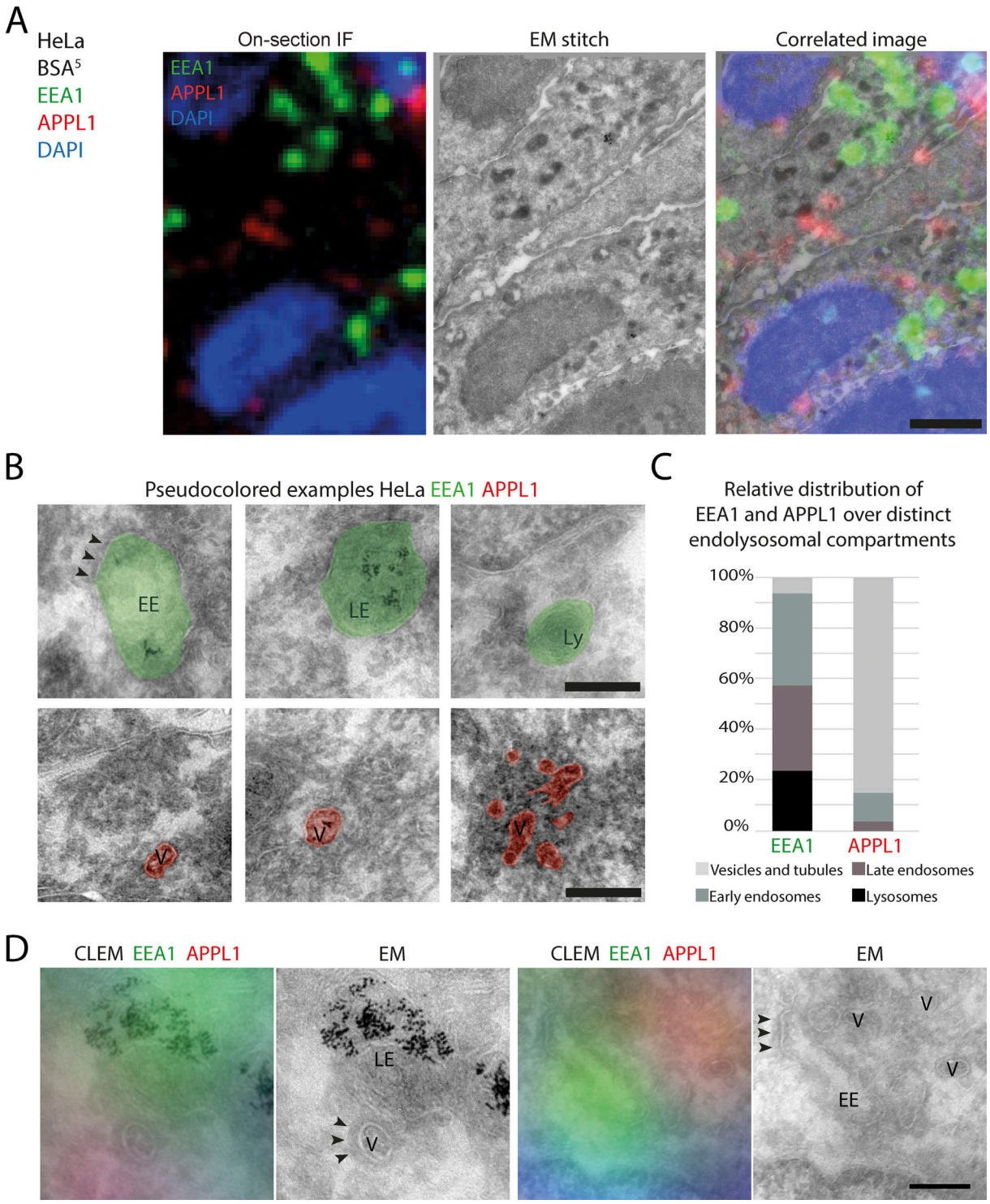

Figure 4. **On-section CLEM of EEA1 and APPL1 endosomes shows strikingly distinct ultrastructures. (A–C)** HeLa cells prepared as in Fig. 3 and labeled for EEA1 and APPL1 with Alexa Fluor 488 and 568, respectively. For uncolored images of B, see Fig. S4 B. **(C)** Relative distribution of EEA1 and APPL1 over distinct endolysosomal compartments identified by morphology. *n* = 92 for EEA1 and 55 for APPL1, taken from three different samples. EEA1 predominantly labels early and late endosomes. APPL1 is almost exclusively found on small vesicles. **(D)** Colocalization of EEA1 and APPL1 is rare. By CLEM, such spots often appear as an early endosomes with nearby vesicles. Arrowheads indicate clathrin coats. EE, early endosome; LE, late endosome; Ly, lysosome; V, vesicle. Scale bar, 2 µm in A; 200 nm in B and D.

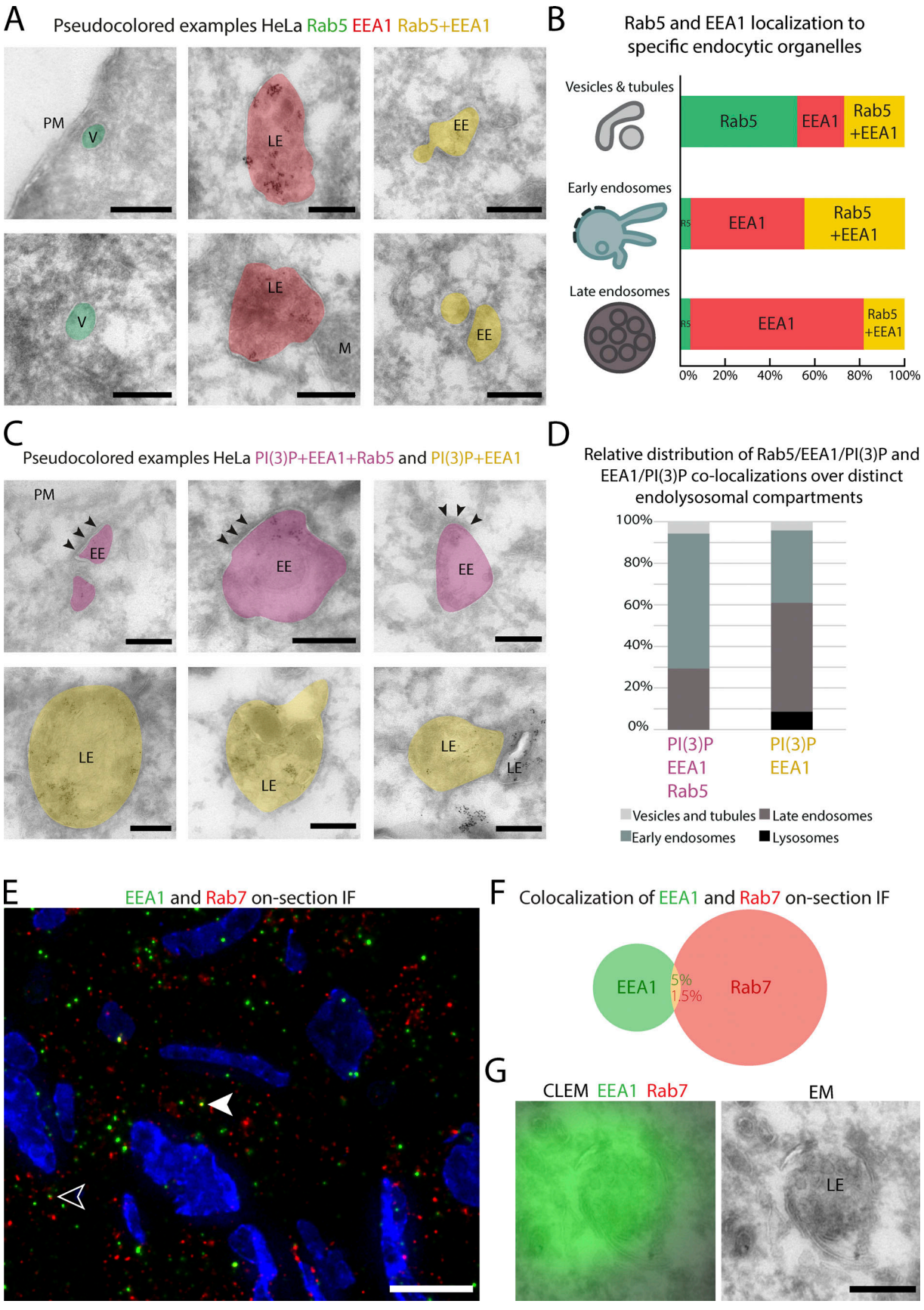

Figure 5. **EEA1 localizes to PI(3)P-positive late endosomes that lack Rab5 and Rab7.** HeLa cells prepared for CLEM as in Fig. 3. **(A)** Pseudocolored CLEM of Rab5 (green) and EEA1 (red) and spots of colocalization in yellow. Original EM images are shown in Fig. S5 A. **(B)** Rab5 and EEA1 distribution per endosomal

subtype. *n* = 40, 76, and 62 Rab5-, EEA1-, and Rab5/EEA1-positive organelles, respectively, collected from three different samples. Most vesicles and tubules contain Rab5 only, most early endosomes contain Rab5/EEA1 or EEA1 only, and most late endosomes contain EEA1 only. **(C)** Representative CLEM images from HeLa cells expressing 2xFYVE-EGFP to label PI(3)P, followed by on-section immunolabeling for Rab5 and EEA1. Rab5/EEA1/PI(3)P-positive organelles are pseudocolored pink, and EEA1/PI(3)P-positive (without Rab5) organelles are yellow. Gold particles in A and C represent internalized BSA[5]. Arrowheads point to clathrin coats. Corresponding original images are shown in Fig. S5 B. **(D)** Relative distributions of Rab5/EEA1/PI(3)P and EEA1/PI(3)P triple and double co-localizations over distinct endolysosomal compartments as identified by morphology. *n* = 17 and 23, respectively, collected from two different samples. Rab5/EEA1/PI(3)P triple colocalization is mostly associated with early endosomes, whereas the majority of Rab5-negative, EEA1/PI(3)P-positive compartments represent late endosomes. **(E)** HeLa cryosection labeled for EEA1 and Rab7 with Alexa Fluor 488 and 568, respectively. Solid arrowhead, false EEA1/Rab7 colocalization that, by CLEM, appeared as a fold in the section (Fig. S6 B). Open arrowhead, closely apposed EEA1 and Rab7 spots that, by CLEM (Fig. S6 C), corresponded to an EEA1-positive early endosome with associated Rab7 vesicles. **(F)** Quantification of Rab7 and EEA1 colocalization on light-microscopy sections. Only 5% of all EEA1 puncta colocalized with Rab7, and only 1.5% of all Rab7 colocalized with EEA1. *n* = 271 cell profiles from three samples. **(G)** Representative CLEM image of an EEA1-positive, Rab7-negative late endosome. EE, early endosome; LE, late endosome; M, mitochondrion; PM, plasma membrane; V, vesicle. IF scale bar, 2 µm; EM scale bars, 200 nm.

correlating hundreds of spots, we show the quantitative localization of different combinations of proteins, with 65–120-nm correlation accuracy and TEM resolution. Moreover, we apply this technology to proteins that cannot be detected by conventional immuno-EM. Thereby we unleash the possibility of ultrastructural localization for an entirely new set of proteins of low abundance or poor antigenicity. We make use of ultrathin cryosections, which are traditionally used for immuno-EM but are also highly compatible with IF imaging. This makes it possible to fluorescently label proteins on-section and subsequently overlay this signal to EM images of the same section. Large datasets are obtained by making stitched, high-magnification images of sections in IF and EM, which contain numerous reference points (e.g., nuclei) for quick and accurate alignment of the datasets (Fig. S3; Mohammadian et al., 2019). We demonstrate the power of our approach by revealing the subcellular distributions of endogenous Rab5, EEA1, APPL1, and Rab7, all key regulatory proteins of the endolysosomal system. Moreover, we combine immunolabeling with the use of a 2xFYVE-EGFP probe to mark PI(3)P. Our data reveal novel information on the spatial distribution of these proteins over distinct endolysosomal compartments, as summarized in Fig. 7, providing new insights in the composition of the endolysosomal system and with consequences for their use as markers for specific endolysosomal compartments.

We show that the proteins under study are detectable by IF but not by immuno-EM using immunogold labeling of cryosections (Fig. 2). Since the primary antibodies for IF and immuno-EM experiments are the same, this discrepancy is likely explained by the differences in labels (fluorescence versus gold) and sample preparation. It has been shown that colloidal gold particles show limited penetration into cryosections (Griffiths and Lucocq, 2014; Griffiths et al., 1993), which predicts a lower SNR than obtained with fluorescent probes penetrating the entire section. Furthermore, the postlabeling approach for EM may result in some loss of antibody–gold complexes, for example during washes in H_2O or postfixation with UA. Labeling for immuno-EM can be enhanced by preembedding labeling, silver enhancement, or peroxidase stains, but these methods affect or obscure morphology, are not quantitative, and limit the number of specific proteins that can be labeled simultaneously.

An important step to enable CLEM studies is to overcome the distinct requirements for fluorescence microscopy (optimized for a high labeling signal) and EM imaging (optimized for high ultrastructural preservation; Murk et al., 2003b; Loussert-Fonta et al., 2020). In general, cross-linking fixatives such as GA decrease antigenicity, as we also observed (Table 2). Furthermore, we found a striking effect of the duration of FA fixation (Table 2). Fixation times longer than 1 h significantly decreased the IF signal for all four proteins under study (Rab5, EEA1, APPL1, and Rab7). As an optimal compromise between fluorescence signal and morphology, we selected a mild fixation of 4% FA for 1 h as the best fixative for CLEM. Although in these conditions EM ultrastructure is not maximally preserved, all defining characteristic features of endolysosomal compartments are readily visible, allowing accurate identification based on their morphology. We suggest testing these conditions for each antigen to be studied by CLEM, by which it is recommended to seek for the strongest fixation possible without significant loss of signal.

Our studies reveal insightful new information on the localization of the four endosomal proteins under study (summarized in Fig. 7). Double-labeling of Rab5 and Rab7 showed a complementary distribution over early and late endosomal compartments, respectively, with very limited overlap. Notably, in HeLa cells, the vast majority of Rab5 (70%) associated with small, 100–200-nm singular endocytic vesicles and tubules rather than with early endosomes (19%). Rab5 is commonly referred to as an early endosome marker. Based on our data, "marker for early endocytic compartments" would be a more correct definition. The relative distribution of Rab5 between distinct early endocytic compartments will vary between cells and different experimental conditions. This is important to keep in mind, since endocytic vesicles and early endosomes are functionally distinct compartments, with early endosomes being complex structures bearing different molecular and functional domains that enable cargo sorting (Geuze et al., 1983; Mari et al., 2008; Sönnichsen et al., 2000; McLauchlan et al., 1998). Rab7 was validated as a suitable and specific marker for late endocytic compartments, which encompassed both late endosomes as well as lysosomes (Figs. 3 D and 7).

Focusing on the Rab5 effectors APPL1 and EEA1, we confirmed by IF that these two proteins mark separate pools of endosomal organelles (Kalaidzidis et al., 2015) and by EM that these represent morphologically distinct membranes (Figs. 4 C and 7). APPL1 is consistently found on small vesicles (APPL1 endosomes) that are mostly oval shaped, 100–150 nm in diameter and length, and sometimes clustered together. By both IF

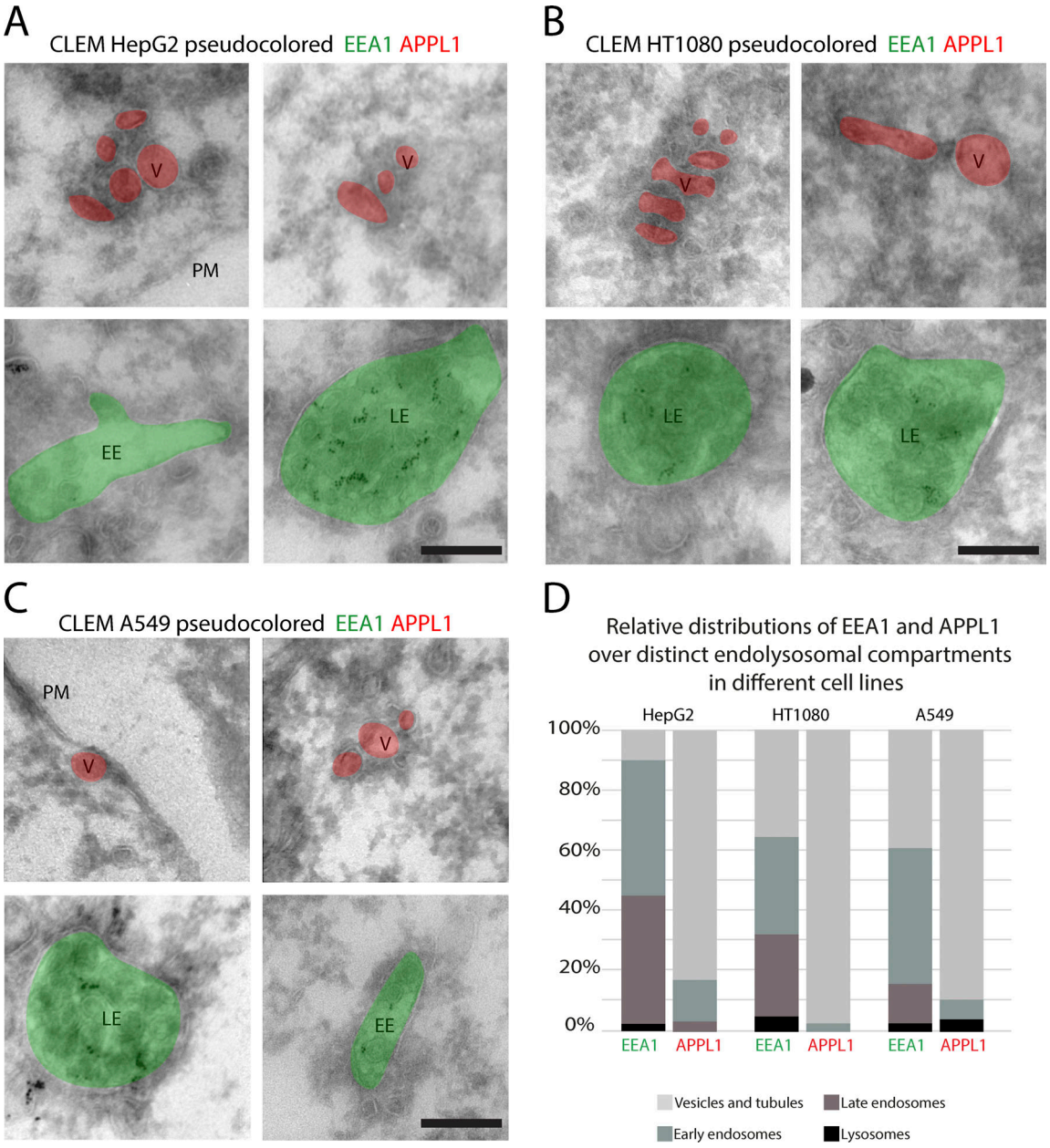

Figure 6. **EEA1 consistently marks early and late endosomes in different cell types.** Indicated cell lines were prepared for CLEM as in Fig. 3. **(A–C)** Pseudocolored EM images based on CLEM of cryosections double-labeled for EEA1 and APPL1. Original images are shown in Fig. S7, A–C. Gold particles represent internalized BSA[5]. **(D)** Relative distributions of EEA1 and APPL1 over distinct endolysosomal compartments as defined by morphology. EEA1 is found on early and late endosomes in all cell lines. APPL1 in all cells predominantly labels small vesicles. HepG2, n = 40 and 29; HT1080, n = 102 and 70; A549, n = 69 and 47 organelles for EEA1 and APPL1, respectively. EE, early endosome; LE, late endosome; PM, plasma membrane; V, vesicle. Scale bars, 200 nm.

and EM (Figs. 1 C and 4 C), we typically found the APPL1-positive vesicles close to the plasma membrane. Apart from an occasional clathrin coat, these endosomes had no distinguishing features, such as tubules or ILVs, nor did they contain any discernable content, except when cells were incubated with BSA[5] before fixation. The consistent association of APPL1 with small, high-curvature vesicles and tubules could be explained by its BAR domain, which promotes membrane curvature (Chial et al., 2008; Habermann, 2004; Mim and Unger, 2012). APPL1 has been proposed to serve as an adaptor or scaffold for membrane receptors and signaling proteins and to regulate cargo sorting and recycling (Kalaidzidis et al., 2015; Diggins and Webb, 2017). How the small APPL1 endosomes accomplish these complex tasks needs to be established. Previous studies show that APPL1 and EEA1 endosomes dynamically interact and can interconvert (Kalaidzidis et al., 2015; Zoncu et al., 2009). Our studies indicate that these interactions are sparse or short-lived, since we found only a very small fraction (5%) of APPL1 colocalizing with EEA1 (Fig. 4 D). By CLEM, these spots often appeared as typical, small APPL1 endosomes close to an EEA1-positive early endosomal vacuole. Overall, EEA1 showed a much wider distribution than APPL1, ranging from

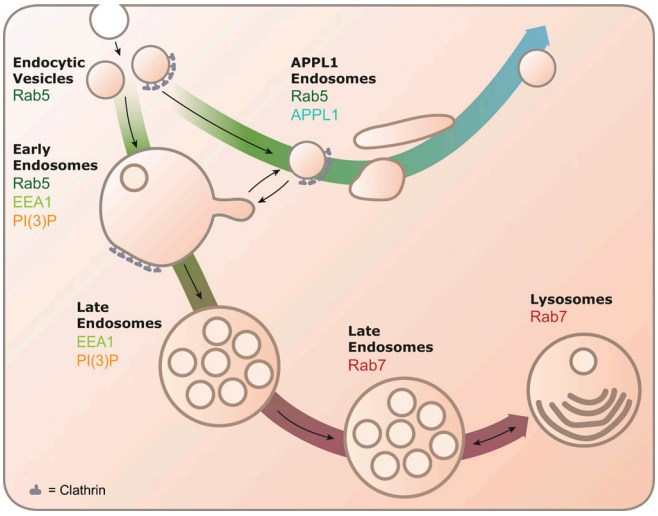

Figure 7. **Schematic summarizing the general localization patterns of Rab5, Rab7, EEA1, APPL1, and PI(3)P as obtained by CLEM.** Rab5 is predominantly found on endocytic vesicles and early endosomes. Rab5 colocalizes with APPL1 on typical tubulo-vesicular APPL1 endosomes. EEA1 and PI(3)P colocalize with Rab5 on early endosomes and without Rab5 on late endosomes that are also negative for Rab7. Rab7 localizes to late endosomes and lysosomes. Larger arrows signify recycling (upper) and degradative (lower) pathways; smaller arrows indicate maturation, vesicle trafficking, or fusion events.

100–150-nm endocytic vesicles to early and late endosomes and even lysosomes (Fig. 4 D).

The most striking finding in our studies is that a significant portion of EEA1 localizes to late endocytic compartments. We found this in Hela cells as well as HepG2, A549, and HT1080 cell lines, albeit with distinct relative distributions. EEA1 is now generally considered a marker for early endosomes. Our data demonstrate that EEA1 actually is a marker for both early and late endosomes. This is important for the functional interpretation of EEA1 IF data, since defining puncta as late rather than early endosomes may significantly change the impact of a dataset. In studies that require specific detection of early endosomes, we recommend double-labeling between EEA1 and Rab5, since the combination of these two markers more specifically labels early endosomes (Fig. 5, A and B).

Correlative imaging of EEA1 with a PI(3)P probe revealed that these markers colocalize on both early and late endosomes: in the case of early endosomes, together with Rab5, and in the case of late endosomes, in the absence of Rab5. These data indicate that after dissociation of Rab5, EEA1 persists on a population of maturing endosomes by binding to PI(3)P. The presence of PI(3)P on late endosomes lacking Rab5 also indicates that conversion to phosphatidylinositol 3,5-bisphosphate can take place after dissociation of Rab5 from endosomes, a finding that is supported by other studies on endosomal maturation (Poteryaev et al., 2010; Huotari and Helenius, 2011; Liu et al., 2017) and recently illustrated by live-cell imaging of EGFP-2xFYVE, which revealed that PI(3)P dissociates after disappearance of Rab5 (Podinovskaia et al., 2021 *Preprint*). The Rab5-negative, EEA1/PI(3)P-positive late endosomes were generally negative for Rab7 (Fig. 5 E), but we occasionally found EEA1-positive late endosomes surrounded by Rab7-positive tubules and vesicles (Fig. S6, C–E-). Although further studies are required to reveal the function of these vesicles, they might represent Rab7/retromer-positive recycling tubules emanating from endosomal vacuoles (Rojas et al., 2008). The existence demonstrated here of a population of EEA1-positive late endosomes without detectable Rab5 and Rab7 indicates a time lag between Rab5 dissociation and Rab7 recruitment to a maturing endosomal vacuole. Endogenous tagging approaches to label simultaneously for Rab5, Rab7, and EEA1 in live cells could be a way to further study this population. In addition, volumetric EM methods can be employed to exclude that Rab5 or Rab7 subdomains are missed on organelles in thin sections (Franke et al., 2019; Fermie et al., 2018).

Concluding, we present a sensitive, quantitative CLEM application to localize endogenous proteins in a morphologic context when classical EM labeling schemes fail, resulting in a refined model of the morpho-functional organization of the endolysosomal system (Fig. 7). Notably, all compartments studied in this paper were selected by IF labeling for CLEM analysis. Hence, nonlabeled compartments were not taken into account, such as for example late endosomes/lysosomes that do not contain Rab7 but Arl8b or Rab9 (Jongsma et al., 2020). Future studies, with additional markers, may lead to the identification of additional endolysosomal compartments or sub-domains. Combined with localization of specific cargo molecules, lipid markers, functional probes, and signaling molecules (e.g., MTORC1), our quantitative CLEM method opens the way toward a detailed morpho-functional understanding of the endolysosomal system in health and disease.

Materials and methods

Cell culture, transfection, and antibodies

HeLa, A549, HepG2, and HT1080 cells were cultured in Corning T-75 cell culture flasks placed in a 5% CO_2 incubator at 37°C. Cells were grown in DMEM supplemented with 10% FCS, 100 U/ml penicillin, and 100 µg/ml streptomycin. For IF of whole cells, cells were seeded on 12-mm coverslips in a 24-well plate. For EM and CLEM samples, cells were grown in 6-cm culture dishes and incubated with BSA[5] particles (Cell Microscopy Core, University Medical Center [UMC] Utrecht) in full DMEM for 3 h before fixation. We obtained the 2xFYVE-EGFP probe from Addgene (plasmid 140047, deposited by Harald Stenmark). For expression of 2xFYVE-EGFP (Gillooly et al., 2000) to label PI(3)P, we transfected HeLa cells at ∼70% confluence using Effectene (301425; Qiagen). 24 h after transfection, cells were processed in the same way as untransfected samples. For information on antibodies used in this study, see Table 1.

IF

Cells on coverslips were fixed with 4% FA for 15 min followed by three PBS washes and permeabilization in Triton X-100 0.1% in PBS for 10 min. Blocking was performed in 1% BSA in PBS for 10 min before incubation with primary antibodies in 1% BSA for 1 h at RT. Coverslips were incubated with secondary antibodies for 30 min at RT and mounted in Prolong Diamond (P36966; Thermo Fisher Scientific) with DAPI.

Samples were imaged at RT on an LSM700 Leica confocal microscope with photomultiplier detector and 63×, 1.4-NA oil objective using Zen software. Images were recorded as single slices with pinhole size at 1 airy unit for each channel. Images were analyzed in Fiji using the ComDet 5.5 plugin (Eugene Katrukha, Cell Biology, Utrecht University) and a custom macro. For the analysis resulting in Fig. 1 G, 124 cells from 2 independent replicates were analyzed, and 102 ± 71 and 391 ± 218 (mean ± SD) particles were found per cell for Rab7 and Rab5, respectively. The percentage of colocalized particles was calculated per cell. For averages and SDs, see Table S1. For Fig. 1 H, 147 cells from 2 independent replicates were analyzed, and 258 ± 154, 119 ± 84, and 106 ± 42 particles were found per cell for Rab7, CD63, and Cathepsin D, respectively. For Fig. 1 I, 352 cells from 2 independent replicates were analyzed, and 121 ± 60, 211 ± 129, and 344 ± 206 particles were found per cell for EEA1, APPL1, and Rab5, respectively.

Sample embedding

For CLEM and Tokuyasu immuno-EM, sample preparation and sectioning were performed as previously described (Möbius and Posthuma, 2019; Slot and Geuze, 2007). A detailed protocol is available in Embedding, cryoprotection, and freezing. In short, cells were fixed by adding 4% FA in 0.1 M phosphate buffer (PB) 1:1 to culture medium to reduce osmotic shock. After 5 min, medium and fixative were replaced with 4% FA in 0.1 M PB for 1 h at RT unless otherwise indicated. Fixative was washed off and quenched with PBS + 0.15% glycine. Cells were detached from the culture dishes using scrapers and collected in PBS with 1% gelatin. After cells were pelleted, 1% gelatin was replaced by 12% gelatin at 37°C and cells were pelleted again. The pellets were solidified on ice, cut into smaller blocks, and infused with 2.3 M sucrose overnight (ON) at 4°C. The smaller blocks were mounted on pins and stored in liquid nitrogen.

The gelatin-embedded cells were cryosectioned to 90-nm-thick sections at −100°C on a DiATOME diamond knife in a Leica ultracut cryomicrotome. Sections were picked up and deposited on formvar- and carbon-coated grids using 2.3 M sucrose and 1.8% methylcellulose (MC) mixed 1:1.

Immuno-EM

We performed the immunolabeling procedure as developed in our laboratory and described in detail in Slot and Geuze (2007). Sections on grids were incubated in PBS at 37°C for ∼30 min to remove the gelatin, 2.3 M sucrose, and 1.8% MC mixture. After washing and blocking steps, we performed labeling using primary antibodies, followed by incubation with bridging antibodies where needed. Grids were then incubated with Protein A conjugated to 10–15-nm gold particles (Cell Microscopy Core, UMC Utrecht). Grids were postfixed for 5 min using 2% UA, pH 7.0, followed by UA/MC mixture, pH 4.0, for 10 min at 4°C. Imaging was performed on a Tecnai T12 TEM using serialEM software.

On-section CLEM procedure

A step-by-step protocol of the CLEM procedure, including reagents and footnotes, is included in Extended method and notes for on-section CLEM. In short, sections on grids were washed using PBS at 37°C for 30 min, followed by short PBS washes, a blocking step, and incubation with primary antibodies for 1 h at RT as described in the previous paragraph. Sections were then incubated with fluorescent secondary antibodies and DAPI for 30 to 90 min. After 30 min, two to three grids were washed in PBS five times, submersed in 50% glycerol, and sandwiched in 50% glycerol between a clean coverslip and slide glass (Waterman-Storer, 2001), sections facing the coverslip. These grids were then imaged at RT on a Leica Thunder fluorescence microscope using a 100×, 1.47-NA oil objective, a Photometrics Prime 95B scientific CMOS camera, and LAS X software. Stitched images were collected, providing a complete view of all sections on a grid. The grids were retrieved by removing the oil from the coverslip and gently dislodging the coverslip from the slide glass. The grids were washed in PBS, and the conventional immuno-EM protocol was resumed with incubation in 1% GA for 5 min, washes in H_2O, and postfixation using UA. We processed only two to three grids at a time from secondary incubation onward to reduce time in 50% glycerol and deterioration of labeling.

After sample preparation for EM, sections were imaged in a Tecnai T12 TEM using serialEM software (Mastronarde, 2018). We selected the regions for EM tileset images based on the fluorescence images of the same section. After acquisition of the EM images, the data were transferred to a workstation computer and stitched together using Etomo montage blending software (Mastronarde and Held, 2017). The stitched EM image tileset and the corresponding fluorescence image were loaded into Adobe Photoshop 2019 and aligned based on DAPI signal and morphology of nuclei. Images were linearly resized, rotated, or moved in x and y axes to achieve best visual overlay. We also performed landmark-based correlation using the ec-CLEM plugin (Paul-Gilloteaux et al., 2017) in Icy software (de Chaumont et al., 2012) to assess the accuracy of our overlays (Fig. S3). The landmarks were again based on DAPI and nuclear morphology and yielded a predicted error of 60–120 nm across the correlated image (Fig. S3 E). Correlated images were exported as TIF files and loaded into Fiji (Schindelin et al., 2012) to select and individually crop organelles. These were categorized based on morphologic criteria, resulting in organelle distributions.

Definition of endolysosomes by EM morphology

A wealth of EM images collected over the last few decades, by many different laboratories and many different methods, has resulted in general morphologic criteria of endolysosomal compartments (e.g., Mari et al., 2008; Peden et al., 2004; Fermie et al., 2018; Klumperman and Raposo, 2014). Based on these collective studies, we here defined early endosomes as irregularly shaped electron-lucent vacuoles containing fewer than six ILVs, often displaying a flat clathrin coat (which contains Hrs) and/or associated tubules; late endosomes as globular shaped vacuoles with a relatively electron-dense content and containing six or more ILVs; lysosomes as vacuoles irregular in shape and size with a variable, mixed content of ILVs, amorphous, electron-dense material, and degraded membranes that can form onion-like concentric rings. This last definition includes

endolysosomes and autolysosomes formed after fusion of lysosomes with late endosomes or autophagosomes. Structures <200 nm in diameter were designated "tubulo-vesicular," since a round profile might represent a cross section of an elongated tubule. Although these categorizations are not absolute, they maximally represent our current knowledge on structure–function relationships and offer an objective tool to compare the distribution of the different endosomal markers using the same criteria.

Extended method and notes for on-section CLEM

We here describe the on-section CLEM procedure and associated protocols in detail to help other researchers use this technique to its full advantage.

Fixation

For most on-section CLEM approaches with immunolabeling, it is preferable to fix cells in 4% FA in 0.1 M PB, pH 7.4, without GA. Although addition of even small percentages (0.05–0.2%) of GA significantly improves the morphology, it has a negative effect on the efficacy of many antibodies. It additionally generates autofluorescent reaction products, which have to be quenched (e.g., with sodium borohydride [$NaBH_4$]) before labeling. Fixation with 4% FA is therefore preferable, the duration of the fixation can be optimized depending on the antibodies used. Generally speaking, longer fixation improves preservation of the ultrastructure, while brief fixation is beneficial for labeling efficacy. We suggest testing durations in a range from 1 h to ON fixation. The performance of the antibody in regular IF can serve as an indicator for how well the antibody will work in CLEM and which fixation is best suited for it.

Embedding, cryoprotection, and freezing

After fixation, cells are scraped, pelleted, and embedded in 12% gelatin. Storage of samples before embedding should be avoided for CLEM, as storage in low-percentage FA (0.5–1.0%) will gradually progress the fixation, while storage in anything else will slowly reverse the fixation and worsen preservation of the ultrastructure.

The following is a step-by-step protocol for sample preparation of adherent cells: For initial fixation, add 4% FA in 0.1 M PB, pH 7.4, to cell culture medium 1:1 for 5 min; replace fixative and medium for 4% FA in 0.1 M PB, pH 7.4, for 1 h to ON (optimize fixation length for best results); wash in PBS 3×; wash in PBS + 0.15% glycine for 10 min; replace with PBS; add prewarmed (37°C) 2% gelatin 1:1 to PBS; scrape cells; transfer to microcentrifuge tube and pellet cells by centrifugation at 6,000 *g* for 1 min; remove supernatant; resuspend cells in prewarmed (37°C) 12% gelatin and infuse cells for 10 min at 37°C; pellet cells by centrifugation at 6,000 *g* for 1 min; solidify gelatin on ice for 30 min; cut microcentrifuge tube above cell pellet; cut tip with pellet in two and infuse with 2.3 M sucrose for 15–30 min to detach cells and gelatin from the plastic of the tube; remove embedded cell pellet from tube and cut into smaller blocks (~1 mm^3); incubate in 2.3 M sucrose ON at 4°C, rotating end over end; place blocks on pins suitable for use in cryo-ultramicrotomes; and snap-freeze and store in liquid nitrogen.

Cryosectioning

Embedded cells are sectioned in a cryo-ultramicrotome. The chamber, knife, and specimen temperatures are set to −100°C. The face of the blocks of gelatin-embedded cells are trimmed to a rectangular shape of ~250 by 375 µm and cut to sections of 90–100-nm thickness. If ON 4% FA fixation is chosen, or GA is added, the temperature can be reduced to −110°C or −120°C to aid in cutting thinner (70–90-nm) sections. Section pickup is best done using a loop dipped in a 1:1 2.3 M sucrose and 1.8% MC mixture. After pickup, the sections are deposited on EM grids coated with formvar and carbon and can be stored for 1–3 d at 4°C before use.

Immunolabeling and CLEM workflow

Step-by-step protocol: Place the grid sections down on PBS in a dish (e.g., a 3-cm Petri dish or multiwell plate) in a 37°C stove for 20–30 min. This removes the sucrose + MC and the 12% gelatin in between the cells; wash the grids on ~100-µl drops of PBS + 0.15% glycine on parafilm at RT 3× for 2 min; perform blocking step in PBS + 0.1% acetylated BSA (BSA-c) + 0.5% cold fish-skin gelatin (FSG) for 10 min; incubate with primary antibody diluted in PBS + 0.1% BSA-c + 0.5% FSG for 60–120 min; wash in PBS + 0.1% BSA-c + 0.5% FSG 5× for 2 min; incubate with fluorescent secondary antibody and DAPI in PBS + 0.1% BSA-c + 0.5% FSG for >20 minutes; wash in PBS + 0.1% BSA-c + 0.5% FSG 5× for 2 min (optional: incubate for 20 min with Protein A-Gold for immunogold labeling; wash in PBS + 0.1% BSA-c + 0.5% FSG 5× for 2 min); wash in PBS 5× for 2 min; wash in demineralized H_2O 3× for 2 min; submerge the grids in 50% glycerol in H_2O; put grids on clean object slide, sections facing up; add a small droplet of glycerol; cover with a clean coverslip; perform imaging of the sections on a suitable fluorescence microscope; remove the sample from the microscope and add H_2O to the 50% glycerol from the sides of the coverslip (this helps loosen the coverslip from the object glass); remove the coverslip and do not let the lens oil contact the glycerol or H_2O; unmount the grids in H_2O; carefully dry the back sides of the grids and do not let the section-holding side dry completely; wash grids on drops of H_2O 2× for 2 min; fix in PB 0.1 M + 1% GA for 5 min; wash in H_2O 10× for 2 min; postfix in 2% UA, pH 7, for 5 min; wash 2× in MC/UA, pH 4, on ice briefly; incubate with MC/UA, pH 4, on ice for 5–10 min; loop out with a metal ring and dab excess MC/UA pH4 on filter paper (this forms a thin layer of MC on the sections); and let the grid dry at RT.

Note: The IF labeling can slowly deteriorate while the grids are kept in 50% glycerol. It is therefore advised to process and image only a few grids at a time, keeping the time between secondary labeling and fixation in 1% GA to 30–45 min. The remaining grids can be left in the secondary labeling step or on DAPI solution until they are ready for processing and imaging. Take care to fully submerge the grids in 50% glycerol, since air trapped between the grids and the coverslip can break the formvar film. The slide glass and coverglass used to sandwich the grid should be thoroughly cleaned beforehand. Use the "squeaky clean coverslips" protocol described by Waterman-Storer (2001). When retrieving the grids from between the slide and coverglass, be careful not to mix the immersion oil

from the microscope with the 50% glycerol, as this might leave oil on the sections. Drying of the back sides of the grids should be performed with care, as complete drying of the grid will result in deterioration of the ultrastructure. For fluorescence imaging, we recommend a wide-field microscope with a fast, automated stage, a sensitive camera, and the ability to make image tilesets. Use a 60–100× oil objective to create high-resolution image tilesets of (parts of) the ribbon of sections. Having a large area imaged in the fluorescence microscope will aid in finding and selecting areas to image with EM. On slower microscopes or larger samples, it is also possible to create a tileset at a lower magnification as an overview, and then select areas of interest for imaging using a higher-magnification objective.

Correlation

To select the area to be imaged in EM, begin by finding a region that has been imaged in fluorescence microscopy. Select an area that has well-preserved ultrastructure in EM and specific, in-focus signal in fluorescence microscopy. For EM imaging, we recommend using a TEM with high image quality at 30,000–100,000× magnification capable of generating image tilesets. In the selected area, generate a tileset at 40,000–50,000× magnification of roughly 500–1000 µm^2. After postprocessing the data to generate a large, continuous EM image, overlay the EM and fluorescence images using software designed for this operation, such as the ec-CLEM plug-in in Icy, or by manually translating the images in suitable software (such as Adobe Photoshop). In either case, use reference points that are not the primary object of study and are available in both EM and fluorescence to overlay your images. These can be edges of nuclei, cell outlines, mitochondria, or specific bimodal probes (fiducial markers), as long as an appropriate marker has been included in the labeling procedure.

Reagents

Reagents used are as follows. PB 0.2 M: made by mixing 0.2 M $NaH_2PO_4.1H_2O$ and 0.2 M $Na_2PO_4.2H_2O$ in 19:81 ratio and dilute as needed; 2.3 M sucrose: Sucrose D(+) saccharose in 0.1 M PB; UA, pH 7: dissolve 4 g UA in 100 ml H_2O, dissolve 3.8 g oxalic acid in 100 ml H_2O, mix 1:1, add NH_4OH until pH 7.0 is reached (use pH indicator sticks), and filter at 0.45 µm before use; MC/UA, pH 4: dissolve 0.4 g UA in 10 ml H_2O and mix 1:9 with 2% cellulose in H_2O; MC: 1.8% MC (25 centipoises, Sigma M-6385) in H_2O; gelatin: for 12%, add 12 g food-grade gelatin to 75 ml of 0.1 M PB, warm to 60°C, stir, add 100 µl of 20% Na-Azide, add 0.1 M PB up to 100 ml, and dilute in 0.1 M PB as needed; FA: for 16% stock aliquots, add 80 g PFA (prilled, 441244; Sigma-Aldrich) to 400 ml H_2O, warm to 60°C. stir for 15 min, add 0.1 M NaOH until pH is 7 (use indicator sticks), stir for 30 min at 60°C, cool to RT, check pH again, add H_2O up to 500 ml, filter solution, freeze aliquots, thaw for use (sometimes heating is required), and do not use if solution does not turn clear; BSA (fraction V, A-9647; Sigma-Aldrich): dilute in H_2O; Protein-A gold (protein-A conjugated to colloidal gold particles): made in-house (Cell Microscopy Core, UMC Utrecht) and available online.

Online supplemental materials

Fig. S1 shows the effect of FA fixation on fluorescence and morphology, and supports Table 2. Fig. S2 shows the effect of GA fixation on fluorescence and morphology, and supports Table 2. Fig. S3 is an overview of registration procedure and accuracy. Fig. S4 shows non-pseudocolored images of Figs. 3 and 4. Fig. S5 shows non-pseudocolored images of Fig. 5. Fig. S6 shows a CLEM overview of PI(3)P and examples of Rab7/EEA1 CLEM, and supports Fig. 5. Fig. S7 shows non-pseudocolored images of Fig. 6. Table S1 lists organelle, colocalization, and SD values for Fig. 1.

Acknowledgments

We thank our colleagues of the Cell Biology section and Centre for Molecular Medicine for fruitful discussions and feedback. We especially thank Prof. Catherine Rabouille for constructive and valuable discussion of the work.

N. Liv is supported by a ZonMw TOP grant (40-00812-98-16006 to J. Klumperman). The EM within this work is part of the research program National Roadmap for Large-Scale Research Infrastructure, which is financed by the Dutch Research Council (project number 184.034.014).

The authors declare no competing financial interests.

Author contributions: Experiments: J. van der Beek, C. de Heus; Study design: J. van der Beek, N. Liv, J. Klumperman; Manuscript writing: J. van der Beek, J. Klumperman; Manuscript reviewing and revision: J. van der Beek, N. Liv, J. Klumperman; Funding and supervision: J. Klumperman.

Submitted: 8 June 2021
Revised: 22 October 2021
Accepted: 1 November 2021

References

Ballabio, A., and J.S. Bonifacino. 2020. Lysosomes as dynamic regulators of cell and organismal homeostasis. *Nat. Rev. Mol. Cell Biol.* 21:101–118. https://doi.org/10.1038/s41580-019-0185-4

Barrett, A.J. 1980. Cathepsin D: The lysosomal aspartic proteinase. *Ciba Found. Symp.* 75:37–50. https://doi.org/10.1002/9780470720585.ch3

Bernhard, W., and C. Rouiller. 1956. Close topographical relationship between mitochondria and ergastoplasm of liver cells in a definite phase of cellular activity. *J. Biophys. Biochem. Cytol.* 2(4, Suppl):73–78. https://doi.org/10.1083/jcb.2.4.73

Biazik, J., P. Ylä-Anttila, H. Vihinen, E. Jokitalo, and E.L. Eskelinen. 2015. Ultrastructural relationship of the phagophore with surrounding organelles. *Autophagy*. 11:439–451. https://doi.org/10.1080/15548627.2015.1017178

Bright, N.A., L.J. Davis, and J.P. Luzio. 2016. Endolysosomes are the principal intracellular sites of acid hydrolase activity. *Curr. Biol.* 26:2233–2245. https://doi.org/10.1016/j.cub.2016.06.046

Bucci, C., P. Thomsen, P. Nicoziani, J. McCarthy, and B. van Deurs. 2000. Rab7: a key to lysosome biogenesis. *Mol. Biol. Cell.* 11:467–480. https://doi.org/10.1091/mbc.11.2.467

Chial, H.J., R. Wu, C.V. Ustach, L.C. McPhail, W.C. Mobley, and Y.Q. Chen. 2008. Membrane targeting by APPL1 and APPL2: dynamic scaffolds that oligomerize and bind phosphoinositides. *Traffic.* 9:215–229. https://doi.org/10.1111/j.1600-0854.2007.00680.x

Cortese, K., G. Vicidomini, M.C. Gagliani, P. Boccacci, A. Diaspro, and C. Tacchetti. 2012. 3D HDO-CLEM: Cellular Compartment Analysis by Correlative Light-Electron Microscopy on Cryosection. *In* Müller-Reichert T., Verkade P., eds. Methods in Cell Biology. Academic Press, Cambridge, MA; 111:95–115.

Cullen, P.J., and F. Steinberg. 2018. To degrade or not to degrade: mechanisms and significance of endocytic recycling. *Nat. Rev. Mol. Cell Biol.* 19:679–696. https://doi.org/10.1038/s41580-018-0053-7

D'Agostino, M., H.J. Risselada, A. Lürick, C. Ungermann, and A. Mayer. 2017. A tethering complex drives the terminal stage of SNARE-dependent

membrane fusion. *Nature.* 551:634–638. https://doi.org/10.1038/nature24469
de Chaumont, F., S. Dallongeville, N. Chenouard, N. Hervé, S. Pop, T. Provoost, V. Meas-Yedid, P. Pankajakshan, T. Lecomte, Y. Le Montagner, et al. 2012. Icy: an open bioimage informatics platform for extended reproducible research. *Nat. Methods.* 9:690–696. https://doi.org/10.1038/nmeth.2075
Diggins, N.L., and D.J. Webb. 2017. APPL1 is a multifunctional endosomal signaling adaptor protein. *Biochem. Soc. Trans.* 45:771–779. https://doi.org/10.1042/BST20160191
Ferguson, S.M. 2019. Neuronal lysosomes. *Neurosci. Lett.* 697:1–9. https://doi.org/10.1016/j.neulet.2018.04.005
Fermie, J., N. Liv, C. Ten Brink, E.G. van Donselaar, W.H. Müller, N.L. Schieber, Y. Schwab, H.C. Gerritsen, and J. Klumperman. 2018. Single organelle dynamics linked to 3D structure by correlative live-cell imaging and 3D electron microscopy. *Traffic.* 19:354–369. https://doi.org/10.1111/tra.12557
Fermie, J., L. de Jager, H. Foster, T. Veenendaal, C. de Heus, S. van Dijk, C. ten Brink, V. Oorschot, L. Yang, W. Li, et al. 2021. Bimodal Endocytic Probe for Three-Dimensional Correlative Light and Electron Microscopy. *bioRxiv*. (Preprint posted August 16, 2021). https://doi.org/10.1101/2021.05.18.444466
Fevrier, B., D. Vilette, F. Archer, D. Loew, W. Faigle, M. Vidal, H. Laude, and G. Raposo. 2004. Cells release prions in association with exosomes. *Proc. Natl. Acad. Sci. USA.* 101:9683–9688. https://doi.org/10.1073/pnas.0308413101
Franke, C., U. Repnik, S. Segeletz, N. Brouilly, Y. Kalaidzidis, J.M. Verbavatz, and M. Zerial. 2019. Correlative single-molecule localization microscopy and electron tomography reveals endosome nanoscale domains. *Traffic.* 20:601–617. https://doi.org/10.1111/tra.12671
Friedman, J.R., L.L. Lackner, M. West, J.R. DiBenedetto, J. Nunnari, and G.K. Voeltz. 2011. ER tubules mark sites of mitochondrial division. *Science.* 334:358–362. https://doi.org/10.1126/science.1207385
Futter, C.E., A. Pearse, L.J. Hewlett, and C.R. Hopkins. 1996. Multivesicular endosomes containing internalized EGF-EGF receptor complexes mature and then fuse directly with lysosomes. *J. Cell Biol.* 132:1011–1023. https://doi.org/10.1083/jcb.132.6.1011
Gao, X., A. De Mazière, D.B. Iaea, C.P. Arthur, J. Klumperman, C. Ciferri, and R.N. Hannoush. 2019. Visualizing the cellular route of entry of a cystine-knot peptide with Xfect transfection reagent by electron microscopy. *Sci. Rep.* 9:6907. https://doi.org/10.1038/s41598-019-43285-5
Gaullier, J.M., A. Simonsen, A. D'Arrigo, B. Bremnes, H. Stenmark, and R. Aasland. 1998. FYVE fingers bind PtdIns(3)P. *Nature.* 394:432–433. https://doi.org/10.1038/28767
Geuze, H.J., J.W. Slot, G.J.A.M. Strous, H.F. Lodish, and A.L. Schwartz. 1983. Intracellular site of asialoglycoprotein receptor-ligand uncoupling: double-label immunoelectron microscopy during receptor-mediated endocytosis. *Cell.* 32:277–287. https://doi.org/10.1016/0092-8674(83)90518-4
Gillooly, D.J., I.C. Morrow, M. Lindsay, R. Gould, N.J. Bryant, J.M. Gaullier, R.G. Parton, and H. Stenmark. 2000. Localization of phosphatidylinositol 3-phosphate in yeast and mammalian cells. *EMBO J.* 19:4577–4588. https://doi.org/10.1093/emboj/19.17.4577
Gillooly, D.J., C. Raiborg, and H. Stenmark. 2003. Phosphatidylinositol 3-phosphate is found in microdomains of early endosomes. *Histochem. Cell Biol.* 120:445–453. https://doi.org/10.1007/s00418-003-0591-7
Griffiths, G., and J.M. Lucocq. 2014. Antibodies for immunolabeling by light and electron microscopy: not for the faint hearted. *Histochem. Cell Biol.* 142:347–360. https://doi.org/10.1007/s00418-014-1263-5
Griffiths, G., R.G. Parton, J. Lucocq, B. van Deurs, D. Brown, J.W. Slot, and H.J. Geuze. 1993. The immunofluorescent era of membrane traffic. *Trends Cell Biol.* 3:214–219. https://doi.org/10.1016/0962-8924(93)90114-G
Gruenberg, J., and H. Stenmark. 2004. The biogenesis of multivesicular endosomes. *Nat. Rev. Mol. Cell Biol.* 5:317–323. https://doi.org/10.1038/nrm1360
Habermann, B. 2004. The BAR-domain family of proteins: a case of bending and binding? *EMBO Rep.* 5:250–255. https://doi.org/10.1038/sj.embor.7400105
Hämälistö, S., and M. Jäättelä. 2016. Lysosomes in cancer-living on the edge (of the cell). *Curr. Opin. Cell Biol.* 39:69–76. https://doi.org/10.1016/j.ceb.2016.02.009
Hoffmann, P.C., T.A.M. Bharat, M.R. Wozny, J. Boulanger, E.A. Miller, and W. Kukulski. 2019. Tricalbins contribute to cellular lipid flux and form curved ER-PM contacts that are bridged by rod-shaped structures. *Dev. Cell.* 51:488–502.e8. https://doi.org/10.1016/j.devcel.2019.09.019
Huotari, J., and A. Helenius. 2011. Endosome maturation. *EMBO J.* 30:3481–3500. https://doi.org/10.1038/emboj.2011.286
Ishida, M., and J.S. Bonifacino. 2019. ARFRP1 functions upstream of ARL1 and ARL5 to coordinate recruitment of distinct tethering factors to the trans-Golgi network. *J. Cell Biol.* 218:3681–3696. https://doi.org/10.1083/jcb.201905097
Jäger, S., C. Bucci, I. Tanida, T. Ueno, E. Kominami, P. Saftig, and E.L. Eskelinen. 2004. Role for Rab7 in maturation of late autophagic vacuoles. *J. Cell Sci.* 117:4837–4848. https://doi.org/10.1242/jcs.01370
Jongsma, M.L., J. Bakker, B. Cabukusta, N. Liv, D. van Elsland, J. Fermie, J.L. Akkermans, C. Kuijl, S.Y. van der Zanden, L. Janssen, et al. 2020. SKIP-HOPS recruits TBC1D15 for a Rab7-to-Arl8b identity switch to control late endosome transport. *EMBO J.* 39:e102301. https://doi.org/10.15252/embj.2019102301
Junutula, J.R., A.M. De Maziére, A.A. Peden, K.E. Ervin, R.J. Advani, S.M. van Dijk, J. Klumperman, and R.H. Scheller. 2004. Rab14 is involved in membrane trafficking between the Golgi complex and endosomes. *Mol. Biol. Cell.* 15:2218–2229. https://doi.org/10.1091/mbc.e03-10-0777
Kalaidzidis, I., M. Miaczynska, M. Brewińska-Olchowik, A. Hupalowska, C. Ferguson, R.G. Parton, Y. Kalaidzidis, and M. Zerial. 2015. APPL endosomes are not obligatory endocytic intermediates but act as stable cargo-sorting compartments. *J. Cell Biol.* 211:123–144. https://doi.org/10.1083/jcb.201311117
Karabiyik, C., M.J. Lee, and D.C. Rubinsztein. 2017. Autophagy impairment in Parkinson's disease. *Essays Biochem.* 61:711–720. https://doi.org/10.1042/EBC20170023
Klumperman, J., and G. Raposo. 2014. The complex ultrastructure of the endolysosomal system. *Cold Spring Harb. Perspect. Biol.* 6:a016857. https://doi.org/10.1101/cshperspect.a016857
Kurgonaite, K., H. Gandhi, T. Kurth, S. Pautot, P. Schwille, T. Weidemann, and C. Bökel. 2015. Essential role of endocytosis for interleukin-4-receptor-mediated JAK/STAT signalling. *J. Cell Sci.* 128:3781–3795. https://doi.org/10.1242/jcs.170969
Langemeyer, L., F. Fröhlich, and C. Ungermann. 2018. Rab GTPase function in endosome and lysosome biogenesis. *Trends Cell Biol.* 28:957–970. https://doi.org/10.1016/j.tcb.2018.06.007
Lawe, D.C., A. Chawla, E. Merithew, J. Dumas, W. Carrington, K. Fogarty, L. Lifshitz, R. Tuft, D. Lambright, and S. Corvera. 2002. Sequential roles for phosphatidylinositol 3-phosphate and Rab5 in tethering and fusion of early endosomes via their interaction with EEA1. *J. Biol. Chem.* 277:8611–8617. https://doi.org/10.1074/jbc.M109239200
Lee, S., Y.C. Tsai, R. Mattera, W.J. Smith, M.S. Kostelansky, A.M. Weissman, J.S. Bonifacino, and J.H. Hurley. 2006. Structural basis for ubiquitin recognition and autoubiquitination by Rabex-5. *Nat. Struct. Mol. Biol.* 13:264–271. https://doi.org/10.1038/nsmb1064
Lie, P.P.Y., and R.A. Nixon. 2019. Lysosome trafficking and signaling in health and neurodegenerative diseases. *Neurobiol. Dis.* 122:94–105. https://doi.org/10.1016/j.nbd.2018.05.015
Liu, T.T., T.S. Gomez, B.K. Sackey, D.D. Billadeau, and C.G. Burd. 2012. Rab GTPase regulation of retromer-mediated cargo export during endosome maturation. *Mol. Biol. Cell.* 23:2505–2515. https://doi.org/10.1091/mbc.e11-11-0915
Liu, K., R. Xing, Y. Jian, Z. Gao, X. Ma, X. Sun, Y. Li, M. Xu, X. Wang, Y. Jing, et al. 2017. WDR91 is a Rab7 effector required for neuronal development. *J. Cell Biol.* 216:3307–3321. https://doi.org/10.1083/jcb.201705151
Loussert-Fonta, C., G. Toullec, A.A. Paraecattil, Q. Jeangros, T. Krueger, S. Escrig, and A. Meibom. 2020. Correlation of fluorescence microscopy, electron microscopy, and NanoSIMS stable isotope imaging on a single tissue section. *Commun. Biol.* 3:362. https://doi.org/10.1038/s42003-020-1095-x
Luzio, J.P., S.R. Gray, and N.A. Bright. 2010. Endosome-lysosome fusion. Biochem. Soc. Trans. 38:1413–1416.
Mari, M., M.V. Bujny, D. Zeuschner, W.J.C.C. Geerts, J. Griffith, C.M. Petersen, P.J. Cullen, J. Klumperman, and H.J. Geuze. 2008. SNX1 defines an early endosomal recycling exit for sortilin and mannose 6-phosphate receptors. *Traffic.* 9:380–393. https://doi.org/10.1111/j.1600-0854.2007.00686.x
Marques, A.R.A., and P. Saftig. 2019. Lysosomal storage disorders - challenges, concepts and avenues for therapy: beyond rare diseases. *J. Cell Sci.* 132:jcs221739. https://doi.org/10.1242/jcs.221739
Marwaha, R., S.B. Arya, D. Jagga, H. Kaur, A. Tuli, and M. Sharma. 2017. The Rab7 effector PLEKHM1 binds Arl8b to promote cargo traffic to lysosomes. *J. Cell Biol.* 216:1051–1070. https://doi.org/10.1083/jcb.201607085
Mastronarde, D.N. 2018. Advanced data acquisition from electron microscopes with SerialEM. *In* Mansfield J., ed. Microscopy and Microanalysis.

Cambridge University Press, Cambridge, UK. 864–865. https://doi.org/10.1017/S1431927618004816
Mastronarde, D.N., and S.R. Held. 2017. Automated tilt series alignment and tomographic reconstruction in IMOD. *J. Struct. Biol.* 197:102–113. https://doi.org/10.1016/j.jsb.2016.07.011
Mattera, R., Y.C. Tsai, A.M. Weissman, and J.S. Bonifacino. 2006. The Rab5 guanine nucleotide exchange factor Rabex-5 binds ubiquitin (Ub) and functions as a Ub ligase through an atypical Ub-interacting motif and a zinc finger domain. *J. Biol. Chem.* 281:6874–6883. https://doi.org/10.1074/jbc.M509939200
McLauchlan, H., J. Newell, N. Morrice, A. Osborne, M. West, and E. Smythe. 1998. A novel role for Rab5-GDI in ligand sequestration into clathrin-coated pits. *Curr. Biol.* 8:34–45. https://doi.org/10.1016/S0960-9822(98)70018-1
Meister, M., S. Bänfer, U. Gärtner, J. Koskimies, M. Amaddii, R. Jacob, and R. Tikkanen. 2017. Regulation of cargo transfer between ESCRT-0 and ESCRT-I complexes by flotillin-1 during endosomal sorting of ubiquitinated cargo. *Oncogenesis.* 6:e344. https://doi.org/10.1038/oncsis.2017.47
Miaczynska, M., S. Christoforidis, A. Giner, A. Shevchenko, S. Uttenweiler-Joseph, B. Habermann, M. Wilm, R.G. Parton, and M. Zerial. 2004. APPL proteins link Rab5 to nuclear signal transduction via an endosomal compartment. *Cell.* 116:445–456. https://doi.org/10.1016/S0092-8674(04)00117-5
Mim, C., and V.M. Unger. 2012. Membrane curvature and its generation by BAR proteins. *Trends Biochem. Sci.* 37:526–533. https://doi.org/10.1016/j.tibs.2012.09.001
Mishra, A., S. Eathiraj, S. Corvera, and D.G. Lambright. 2010. Structural basis for Rab GTPase recognition and endosome tethering by the C2H2 zinc finger of Early Endosomal Autoantigen 1 (EEA1). *Proc. Natl. Acad. Sci. USA.* 107:10866–10871. https://doi.org/10.1073/pnas.1000843107
Möbius, W., and G. Posthuma. 2019. Sugar and ice: Immunoelectron microscopy using cryosections according to the Tokuyasu method. *Tissue Cell.* 57:90–102. https://doi.org/10.1016/j.tice.2018.08.010
Mohammadian, S., J. Fokkema, A.V. Agronskaia, N. Liv, C. de Heus, E. van Donselaar, G.A. Blab, J. Klumperman, and H.C. Gerritsen. 2019. High accuracy, fiducial marker-based image registration of correlative microscopy images. *Sci. Rep.* 9:3211. https://doi.org/10.1038/s41598-019-40098-4
Mohrmann, K., L. Gerez, V. Oorschot, J. Klumperman, and P. van der Sluijs. 2002. Rab4 function in membrane recycling from early endosomes depends on a membrane to cytoplasm cycle. *J. Biol. Chem.* 277:32029–32035. https://doi.org/10.1074/jbc.M203064200
Mu, F.T., J.M. Callaghan, O. Steele-Mortimer, H. Stenmark, R.G. Parton, P.L. Campbell, J. McCluskey, J.P. Yeo, E.P.C. Tock, and B.H. Toh. 1995. EEA1, an early endosome-associated protein. EEA1 is a conserved alpha-helical peripheral membrane protein flanked by cysteine "fingers" and contains a calmodulin-binding IQ motif. *J. Biol. Chem.* 270:13503–13511. https://doi.org/10.1074/jbc.270.22.13503
Murk, J.L.A.N., B.M. Humbel, U. Ziese, J.M. Griffith, G. Posthuma, J.W. Slot, A.J. Koster, A.J. Verkleij, H.J. Geuze, and M.J. Kleijmeer. 2003a. Endosomal compartmentalization in three dimensions: implications for membrane fusion. *Proc. Natl. Acad. Sci. USA.* 100:13332–13337. https://doi.org/10.1073/pnas.2232379100
Murk, J.L.A.N., G. Posthuma, A.J. Koster, H.J. Geuze, A.J. Verkleij, M.J. Kleijmeer, and B.M. Humbel. 2003b. Influence of aldehyde fixation on the morphology of endosomes and lysosomes: quantitative analysis and electron tomography. *J. Microsc.* 212:81–90. https://doi.org/10.1046/j.1365-2818.2003.01238.x
Murray, D.H., M. Jahnel, J. Lauer, M.J. Avellaneda, N. Brouilly, A. Cezanne, H. Morales-Navarrete, E.D. Perini, C. Ferguson, A.N. Lupas, et al. 2016. An endosomal tether undergoes an entropic collapse to bring vesicles together. *Nature.* 537:107–111. https://doi.org/10.1038/nature19326
Ohya, T., M. Miaczynska, U. Coskun, B. Lommer, A. Runge, D. Drechsel, Y. Kalaidzidis, and M. Zerial. 2009. Reconstitution of Rab- and SNARE-dependent membrane fusion by synthetic endosomes. *Nature.* 459:1091–1097. https://doi.org/10.1038/nature08107
Oorschot, V.M.J., T.E. Sztal, R.J. Bryson-Richardson, and G. Ramm. 2014. Immuno correlative light and electron microscopy on tokuyasu cryosections. *In* Müller-Reichert T., Verkade, P., eds. Methods in Cell Biology. Academic Press, Cambridge, MA; 124:241–258.
Paul-Gilloteaux, P., X. Heiligenstein, M. Belle, M.C. Domart, B. Larijani, L. Collinson, G. Raposo, and J. Salamero. 2017. eC-CLEM: flexible multidimensional registration software for correlative microscopies. *Nat. Methods.* 14:102–103. https://doi.org/10.1038/nmeth.4170
Peden, A.A., V. Oorschot, B.A. Hesser, C.D. Austin, R.H. Scheller, and J. Klumperman. 2004. Localization of the AP-3 adaptor complex defines a novel endosomal exit site for lysosomal membrane proteins. *J. Cell Biol.* 164:1065–1076. https://doi.org/10.1083/jcb.200311064
Pfeffer, S.R. 2017. Rab GTPases: master regulators that establish the secretory and endocytic pathways. *Mol. Biol. Cell.* 28:712–715. https://doi.org/10.1091/mbc.e16-10-0737
Platt, F.M., A. d'Azzo, B.L. Davidson, E.F. Neufeld, and C.J. Tifft. 2018. Lysosomal storage diseases. *Nat. Rev. Dis. Primers.* 4:27. https://doi.org/10.1038/s41572-018-0025-4
Ploper, D., V.F. Taelman, L. Robert, B.S. Perez, B. Titz, H.-W. Chen, T.G. Graeber, E. von Euw, A. Ribas, and E.M. De Robertis. 2015. MITF drives endolysosomal biogenesis and potentiates Wnt signaling in melanoma cells. *Proc. Natl. Acad. Sci. USA.* 112:E420–E429. https://doi.org/10.1073/pnas.1424576112
Podinovskaia, M., C. Prescianotto-Baschong, D.P. Buser, and A. Spang. 2021. A novel live cell imaging assay reveals regulation of endosome maturation. *bioRxiv*. (Preprint posted May 18, 2021). https://doi.org/10.1101/2021.06.28.450147
Pols, M.S., and J. Klumperman. 2009. Trafficking and function of the tetraspanin CD63. *Exp. Cell Res.* 315:1584–1592. https://doi.org/10.1016/j.yexcr.2008.09.020
Poteryaev, D., S. Datta, K. Ackema, M. Zerial, and A. Spang. 2010. Identification of the switch in early-to-late endosome transition. *Cell.* 141:497–508. https://doi.org/10.1016/j.cell.2010.03.011
Puertollano, R., and J.S. Bonifacino. 2004. Interactions of GGA3 with the ubiquitin sorting machinery. *Nat. Cell Biol.* 6:244–251. https://doi.org/10.1038/ncb1106
Raiborg, C., K.G. Bache, A. Mehlum, E. Stang, and H. Stenmark. 2001. Hrs recruits clathrin to early endosomes. *EMBO J.* 20:5008–5021. https://doi.org/10.1093/emboj/20.17.5008
Raiborg, C., T.E. Rusten, and H. Stenmark. 2003. Protein sorting into multivesicular endosomes. *Curr. Opin. Cell Biol.* 15:446–455. https://doi.org/10.1016/S0955-0674(03)00080-2
Raiborg, C., J. Wesche, L. Malerød, and H. Stenmark. 2006. Flat clathrin coats on endosomes mediate degradative protein sorting by scaffolding Hrs in dynamic microdomains. *J. Cell Sci.* 119:2414–2424. https://doi.org/10.1242/jcs.02978
Reggiori, F., and J. Klumperman. 2016. Lysosome Biogenesis and Autophagy. *In* Maxfield F.R., Willard J.M., Lu S., eds. Lysosomes: Biology, Diseases, and Therapeutics. John Wiley & Sons, Inc., Hoboken, NJ. 7–31. https://doi.org/10.1002/9781118978320.ch2
Rink, J., E. Ghigo, Y. Kalaidzidis, and M. Zerial. 2005. Rab conversion as a mechanism of progression from early to late endosomes. *Cell.* 122:735–749. https://doi.org/10.1016/j.cell.2005.06.043
Rocha, N., C. Kuijl, R. van der Kant, L. Janssen, D. Houben, H. Janssen, W. Zwart, and J. Neefjes. 2009. Cholesterol sensor ORP1L contacts the ER protein VAP to control Rab7-RILP-p150 Glued and late endosome positioning. *J. Cell Biol.* 185:1209–1225. https://doi.org/10.1083/jcb.200811005
Rojas, R., T. van Vlijmen, G.A. Mardones, Y. Prabhu, A.L. Rojas, S. Mohammed, A.J.R. Heck, G. Raposo, P. van der Sluijs, and J.S. Bonifacino. 2008. Regulation of retromer recruitment to endosomes by sequential action of Rab5 and Rab7. *J. Cell Biol.* 183:513–526. https://doi.org/10.1083/jcb.200804048
Sachse, M., G. Ramm, G. Strous, and J. Klumperman. 2002a. Endosomes: Multipurpose designs for integrating housekeeping and specialized tasks. Histochem. Cell Biol. 117:91–104.
Sachse, M., S. Urbé, V. Oorschot, G.J. Strous, and J. Klumperman. 2002b. Bilayered clathrin coats on endosomal vacuoles are involved in protein sorting toward lysosomes. *Mol. Biol. Cell.* 13:1313–1328. https://doi.org/10.1091/mbc.01-10-0525
Schindelin, J., I. Arganda-Carreras, E. Frise, V. Kaynig, M. Longair, T. Pietzsch, S. Preibisch, C. Rueden, S. Saalfeld, B. Schmid, et al. 2012. Fiji: an open-source platform for biological-image analysis. *Nat. Methods.* 9:676–682. https://doi.org/10.1038/nmeth.2019
Schwartz, M.L., D.P. Nickerson, B.T. Lobingier, R.L. Plemel, M. Duan, C.G. Angers, M. Zick, and A.J. Merz. 2017. Sec17 (α-SNAP) and an SM-tethering complex regulate the outcome of SNARE zippering in vitro and in vivo. *eLife.* 6:e27396. https://doi.org/10.7554/eLife.27396
Simonsen, A., R. Lippé, S. Christoforidis, J.M. Gaullier, A. Brech, J. Callaghan, B.H. Toh, C. Murphy, M. Zerial, and H. Stenmark. 1998. EEA1 links PI(3)K function to Rab5 regulation of endosome fusion. *Nature.* 394:494–498. https://doi.org/10.1038/28879
Slot, J.W., and H.J. Geuze. 2007. Cryosectioning and immunolabeling. *Nat. Protoc.* 2:2480–2491. https://doi.org/10.1038/nprot.2007.365

Sneeggen, M., N.M. Pedersen, C. Campsteijn, E.M. Haugsten, H. Stenmark, and K.O. Schink. 2019. WDFY2 restrains matrix metalloproteinase secretion and cell invasion by controlling VAMP3-dependent recycling. *Nat. Commun.* 10:2850. https://doi.org/10.1038/s41467-019-10794-w

Song, H., A.S. Orr, M. Lee, M.E. Harner, and W.T. Wickner. 2020. HOPS recognizes each SNARE, assembling ternary *trans*-complexes for rapid fusion upon engagement with the 4th SNARE. *eLife.* 9:e53559. https://doi.org/10.7554/eLife.53559

Sönnichsen, B., S. De Renzis, E. Nielsen, J. Rietdorf, and M. Zerial. 2000. Distinct membrane domains on endosomes in the recycling pathway visualized by multicolor imaging of Rab4, Rab5, and Rab11. *J. Cell Biol.* 149:901–914. https://doi.org/10.1083/jcb.149.4.901

Stenmark, H., R. Aasland, B.H. Toh, and A. D'Arrigo. 1996. Endosomal localization of the autoantigen EEA1 is mediated by a zinc-binding FYVE finger. *J. Biol. Chem.* 271:24048–24054. https://doi.org/10.1074/jbc.271.39.24048

Stoorvogel, W., G.J. Strous, H.J. Geuze, V. Oorschot, and A.L. Schwartz. 1991. Late endosomes derive from early endosomes by maturation. *Cell.* 65: 417–427. https://doi.org/10.1016/0092-8674(91)90459-C

Stroupe, C., C.M. Hickey, J. Mima, A.S. Burfeind, and W. Wickner. 2009. Minimal membrane docking requirements revealed by reconstitution of Rab GTPase-dependent membrane fusion from purified components. *Proc. Natl. Acad. Sci. USA.* 106:17626–17633. https://doi.org/10.1073/pnas.0903801106

van der Beek, J., C. Jonker, R. van der Welle, N. Liv, and J. Klumperman. 2019. CORVET, CHEVI and HOPS - multisubunit tethers of the endo-lysosomal system in health and disease. *J. Cell Sci.* 132:jcs189134. https://doi.org/10.1242/jcs.189134

van Meel, E., and J. Klumperman. 2008. Imaging and imagination: understanding the endo-lysosomal system. *Histochem. Cell Biol.* 129:253–266. https://doi.org/10.1007/s00418-008-0384-0

Vanlandingham, P.A., and B.P. Ceresa. 2009. Rab7 regulates late endocytic trafficking downstream of multivesicular body biogenesis and cargo sequestration. *J. Biol. Chem.* 284:12110–12124. https://doi.org/10.1074/jbc.M809277200

Vicidomini, G., M.C. Gagliani, M. Canfora, K. Cortese, F. Frosi, C. Santangelo, P.P. Di Fiore, P. Boccacci, A. Diaspro, and C. Tacchetti. 2008. High data output and automated 3D correlative light-electron microscopy method. *Traffic.* 9:1828–1838. https://doi.org/10.1111/j.1600-0854.2008.00815.x

Vogel, G.F., H.L. Ebner, M.E.G. de Araujo, T. Schmiedinger, O. Eiter, H. Pircher, K. Gutleben, B. Witting, D. Teis, L.A. Huber, and M.W. Hess. 2015. Ultrastructural morphometry points to a new role for LAMTOR2 in regulating the endo/lysosomal system. *Traffic.* 16:617–634. https://doi.org/10.1111/tra.12271

Vonderheit, A., and A. Helenius. 2005. Rab7 associates with early endosomes to mediate sorting and transport of Semliki forest virus to late endosomes. *PLoS Biol.* 3:e233. https://doi.org/10.1371/journal.pbio.0030233

Waterman-Storer, C.M. 2001. Microtubule/Organelle Motility Assays. Curr. Protoc. Cell Biol. 00:13.1.1–13.1.21.

Willingham, M.C., J.A. Hanover, R.B. Dickson, and I. Pastan. 1984. Morphologic characterization of the pathway of transferrin endocytosis and recycling in human KB cells. *Proc. Natl. Acad. Sci. USA.* 81:175–179. https://doi.org/10.1073/pnas.81.1.175

Wilson, J.M., M. de Hoop, N. Zorzi, B.H. Toh, C.G. Dotti, and R.G. Parton. 2000. EEA1, a tethering protein of the early sorting endosome, shows a polarized distribution in hippocampal neurons, epithelial cells, and fibroblasts. *Mol. Biol. Cell.* 11:2657–2671. https://doi.org/10.1091/mbc.11.8.2657

Yang, C., and X. Wang. 2021. Lysosome biogenesis: Regulation and functions. *J. Cell Biol.* 220:e202102001. https://doi.org/10.1083/jcb.202102001

Zhu, G., J. Chen, J. Liu, J.S. Brunzelle, B. Huang, N. Wakeham, S. Terzyan, X. Li, Z. Rao, G. Li, and X.C. Zhang. 2007. Structure of the APPL1 BAR-PH domain and characterization of its interaction with Rab5. *EMBO J.* 26: 3484–3493. https://doi.org/10.1038/sj.emboj.7601771

Zoncu, R., R.M. Perera, D.M. Balkin, M. Pirruccello, D. Toomre, and P. De Camilli. 2009. A phosphoinositide switch controls the maturation and signaling properties of APPL endosomes. *Cell.* 136:1110–1121. https://doi.org/10.1016/j.cell.2009.01.032

Supplemental material

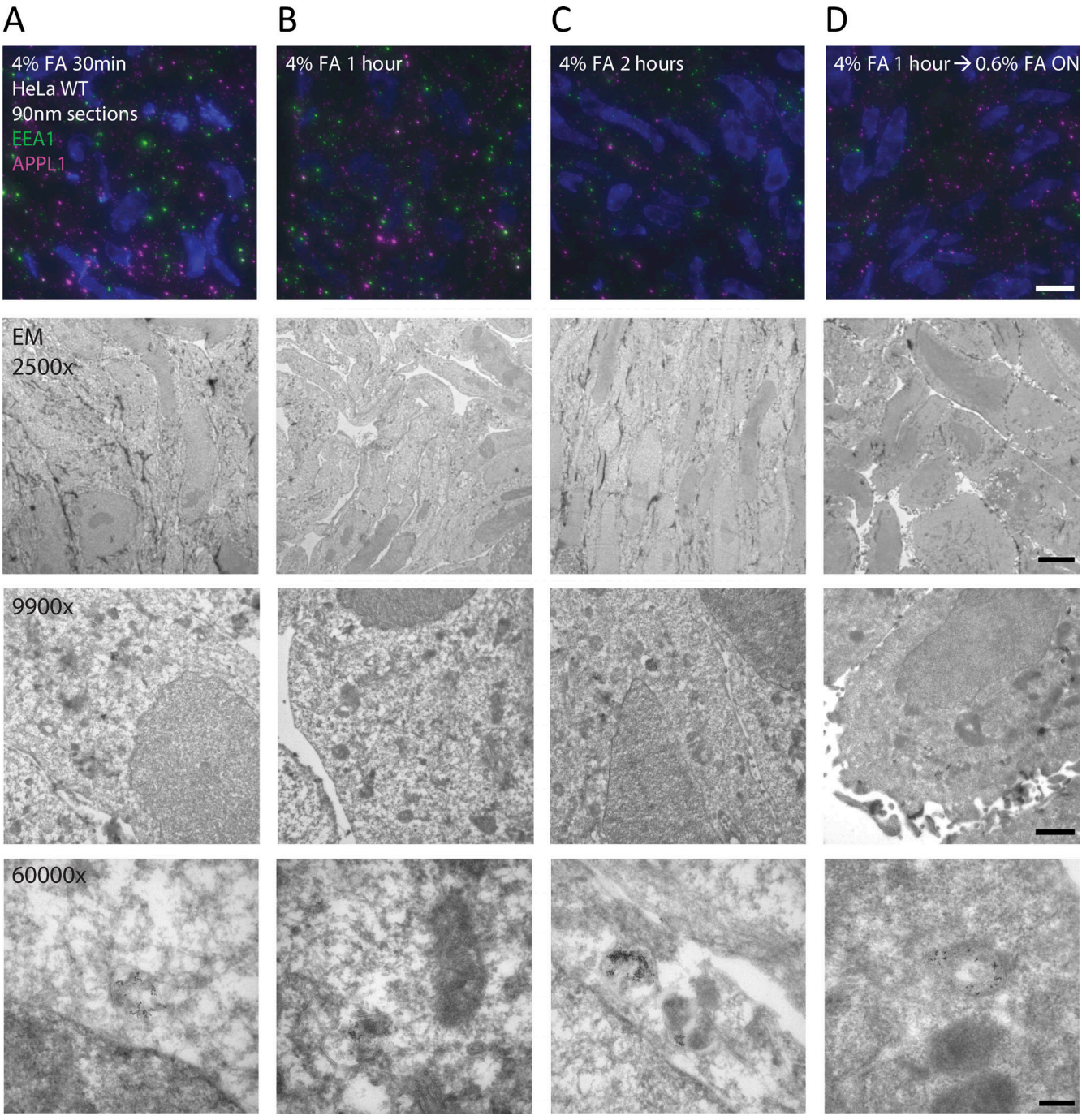

Figure S1. **Effect of prolonged FA fixation on IF signal and EM morphology.** Wide-field microscopy (upper row) and EM images of 90-nm ultrathin cryosections prepared from HeLa cells fixed according to indicated protocols. Sections were fluorescently labeled for EEA1 and APPL1 (upper row) or directly prepared for EM. Over 1 h, FA fixation significantly reduces fluorescent signal. IF images are presented with identical intensity threshold settings. See Table 2 for quantifications of fluorescence microscopy SNR and EM morphology. IF scale bar, 10 µm; EM 2,500× scale bar, 5 µm; 9,900× scale bar, 1 µm; 60,000× scale bar, 200 nm.

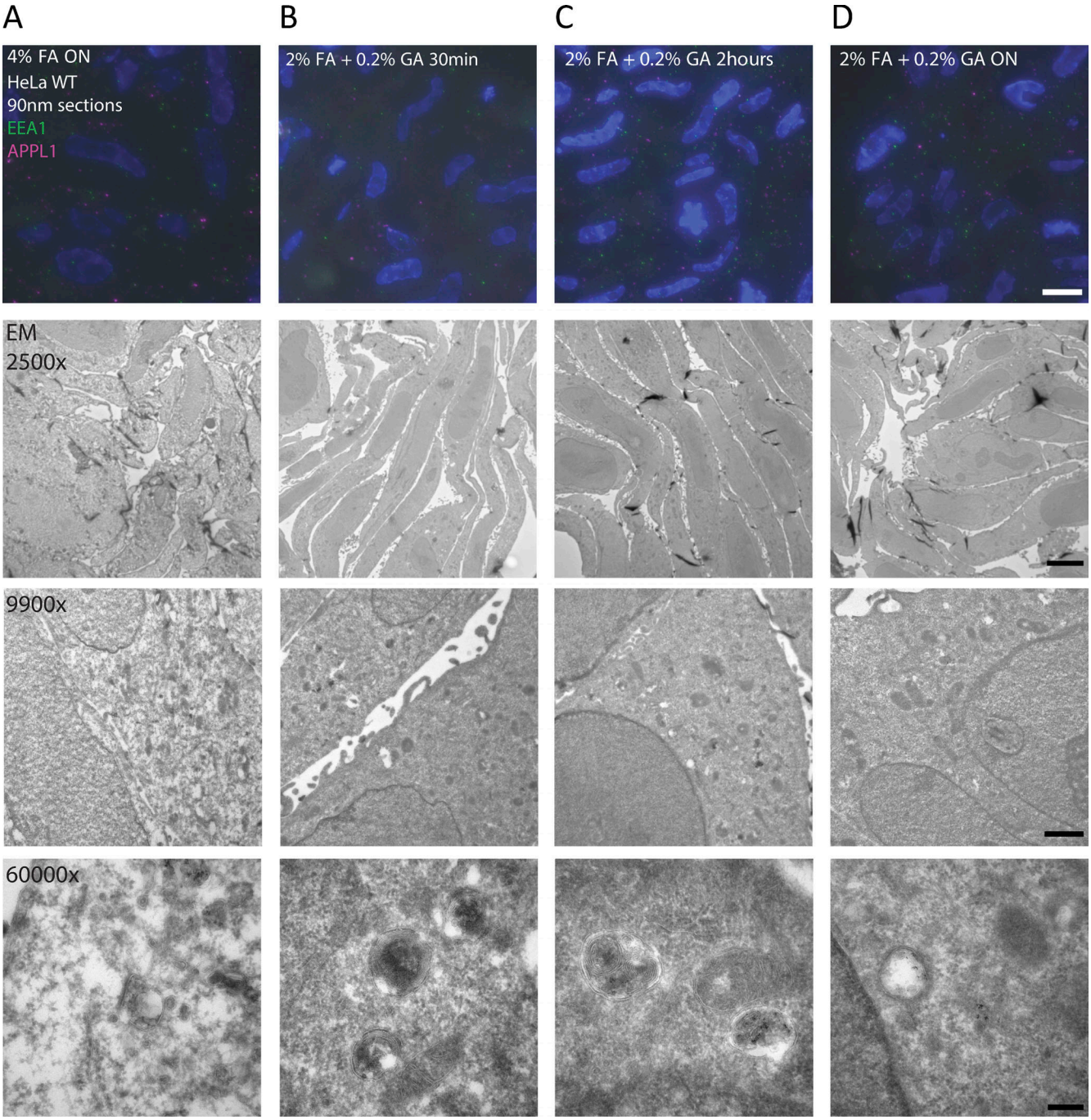

Figure S2. **Effect of GA fixation on IF signal and EM morphology.** Wide-field microscopy and EM images of 90-nm ultrathin cryosections prepared from HeLa cells fixed according to indicated protocols. Sections were fluorescently labeled for EEA1 and APPL1 or directly prepared for EM. GA fixation greatly improves EM morphology but averts the immunofluorescent signal. IF images are presented with identical intensity threshold settings. See Table 2 for quantifications of fluorescence microscopy SNR and EM morphology. IF scale bar, 10 µm; EM 2,500× scale bar, 5 µm; 9,900× scale bar, 1 µm; 60,000× scale bar, 200 nm.

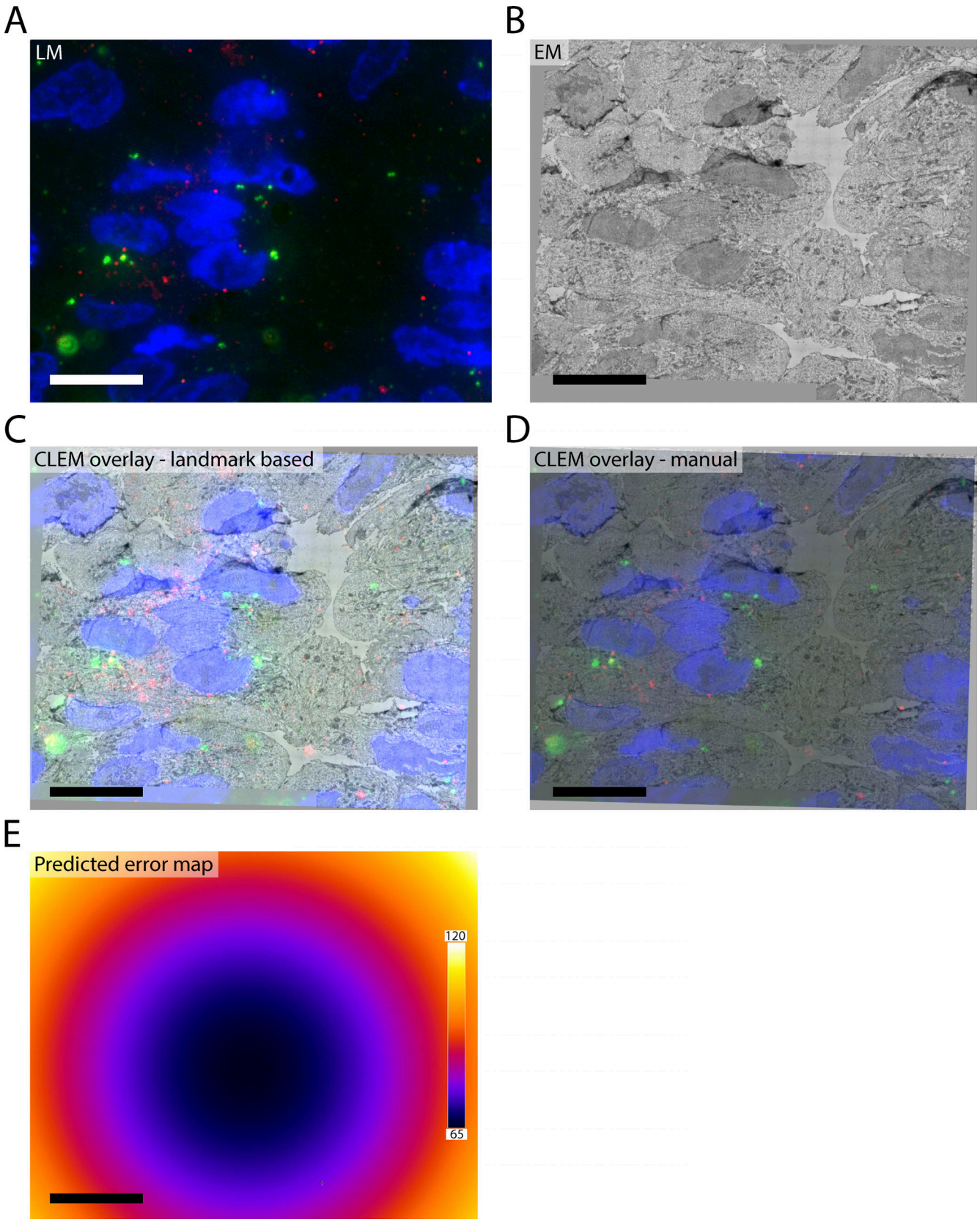

Figure S3. **Correlation accuracy of IF to EM overlays. (A and B)** IF (A) and EM (B) of the same area of HeLa 90-nm cryosections labeled for EEA1 (green) and APPL1 (red). **(C)** Overlay of IF and EM based on landmarks selected on DAPI and nuclear morphology using the ec-CLEM plugin in Icy. **(D)** Overlay based on best visual match of DAPI and nuclear morphology. Both methods yield very similar results. **(E)** Predicted error map of overlay from C. The center of the image is accurately overlaid with a 65-nm error margin, and the edges with a 120-nm error margin. LM, light microscopy. Scale bars, 10 µm.

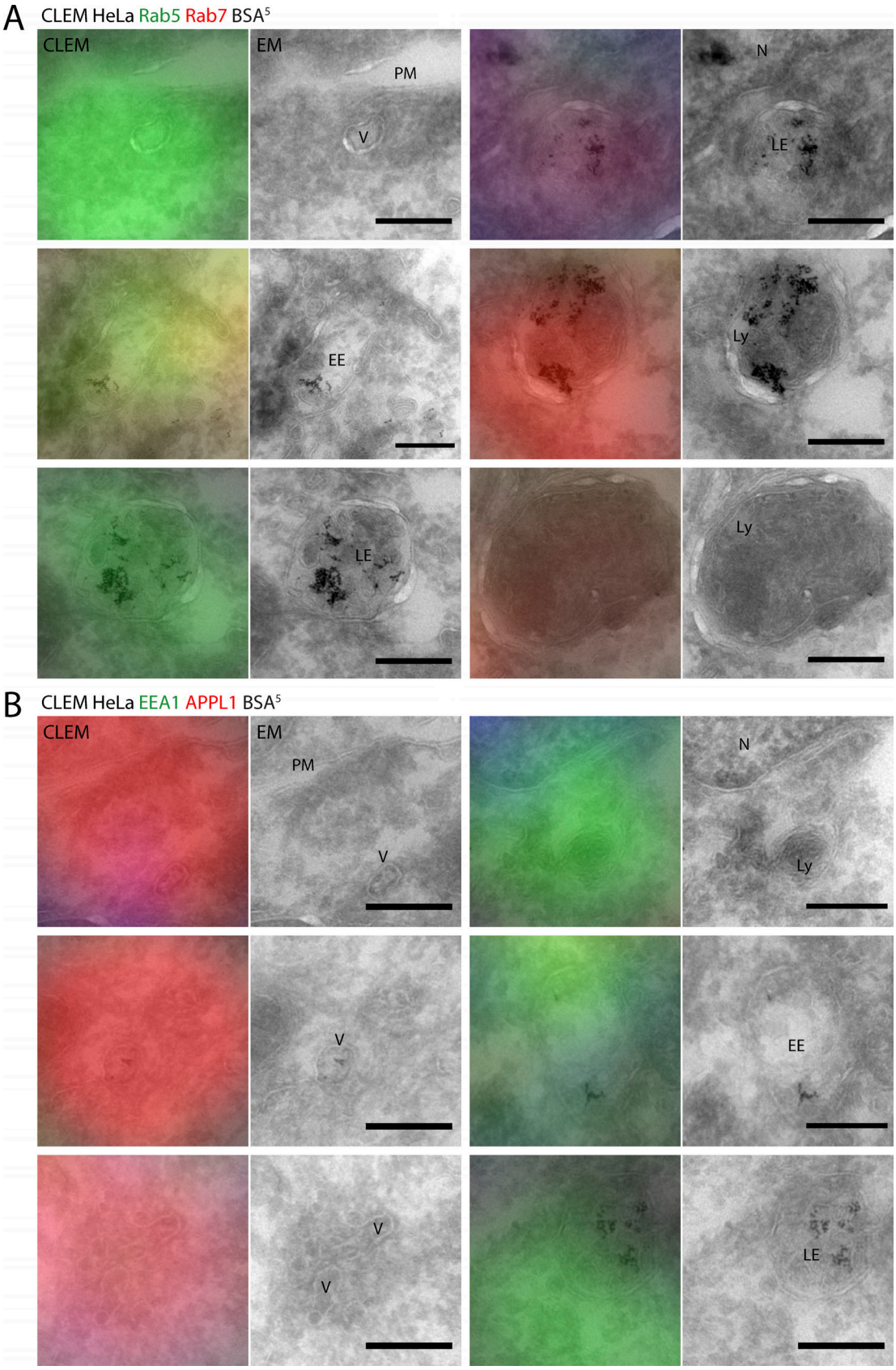

Figure S4. **Original CLEM and EM images from pseudocolored examples in Figs. 3 and 4. (A)** Preparation of samples as described in Fig. 3. Original CLEM and EM images from Fig. 3 C. **(B)** Preparation of samples as described in Fig. 4. CLEM and EM images of Fig. 4 B. EE, early endosome; LE, late endosome; Ly, lysosome; N, nucleus; PM, plasma membrane; V, vesicle. Scale bars, 200 nm.

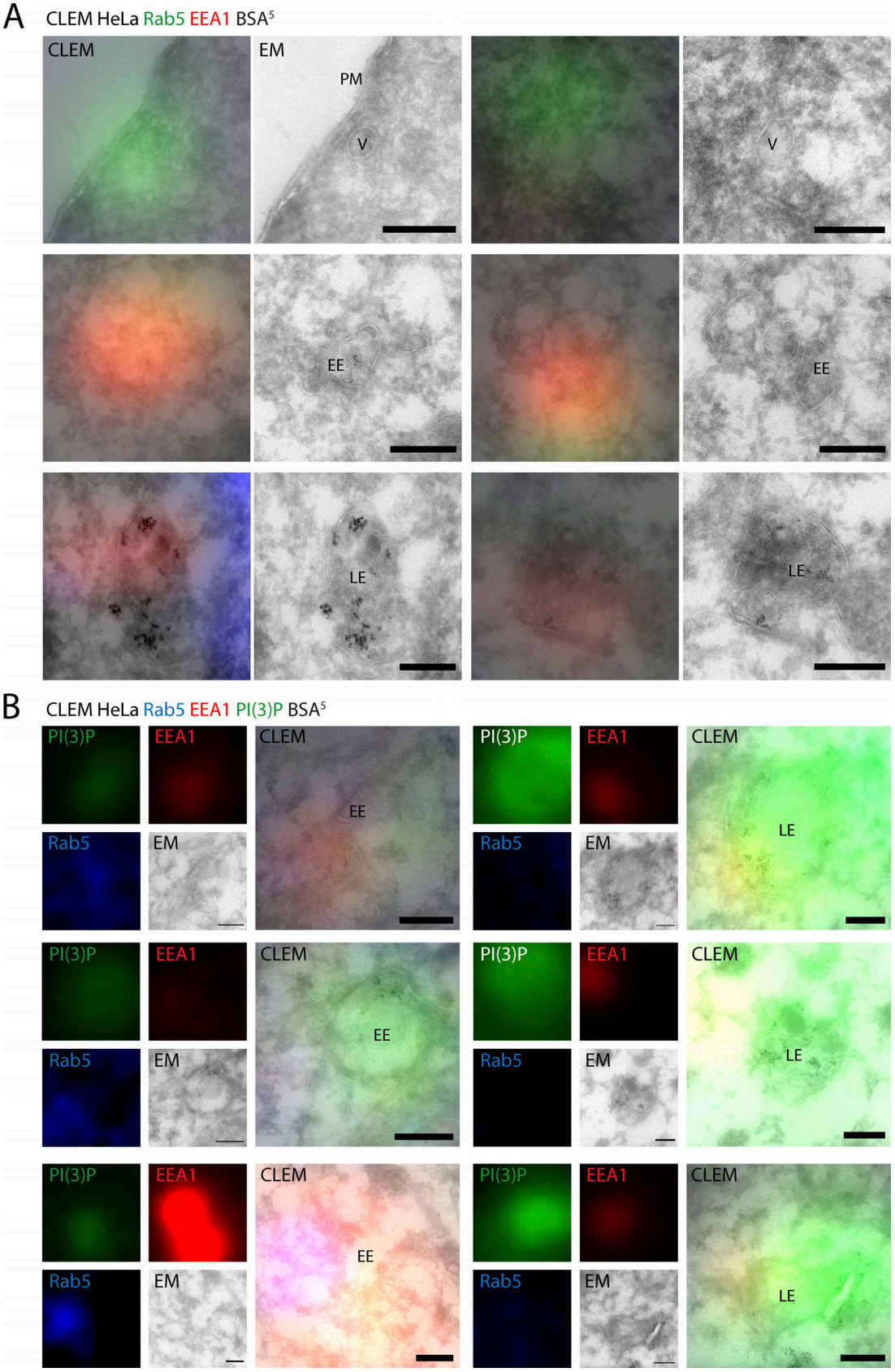

Figure S5. **Original CLEM and EM images from pseudocolored examples in Fig. 5. (A and B)** Preparation of samples as described in Fig. 5. **(A)** Original CLEM and EM images from pseudocolored examples in Fig. 5 A. **(B)** Original CLEM, EM, and single-channel FM images of pseudocolored examples in Fig. 5 C. EE, early endosome; LE, late endosomes; PM, plasma membrane; V, vesicle. Scale bars, 200 nm.

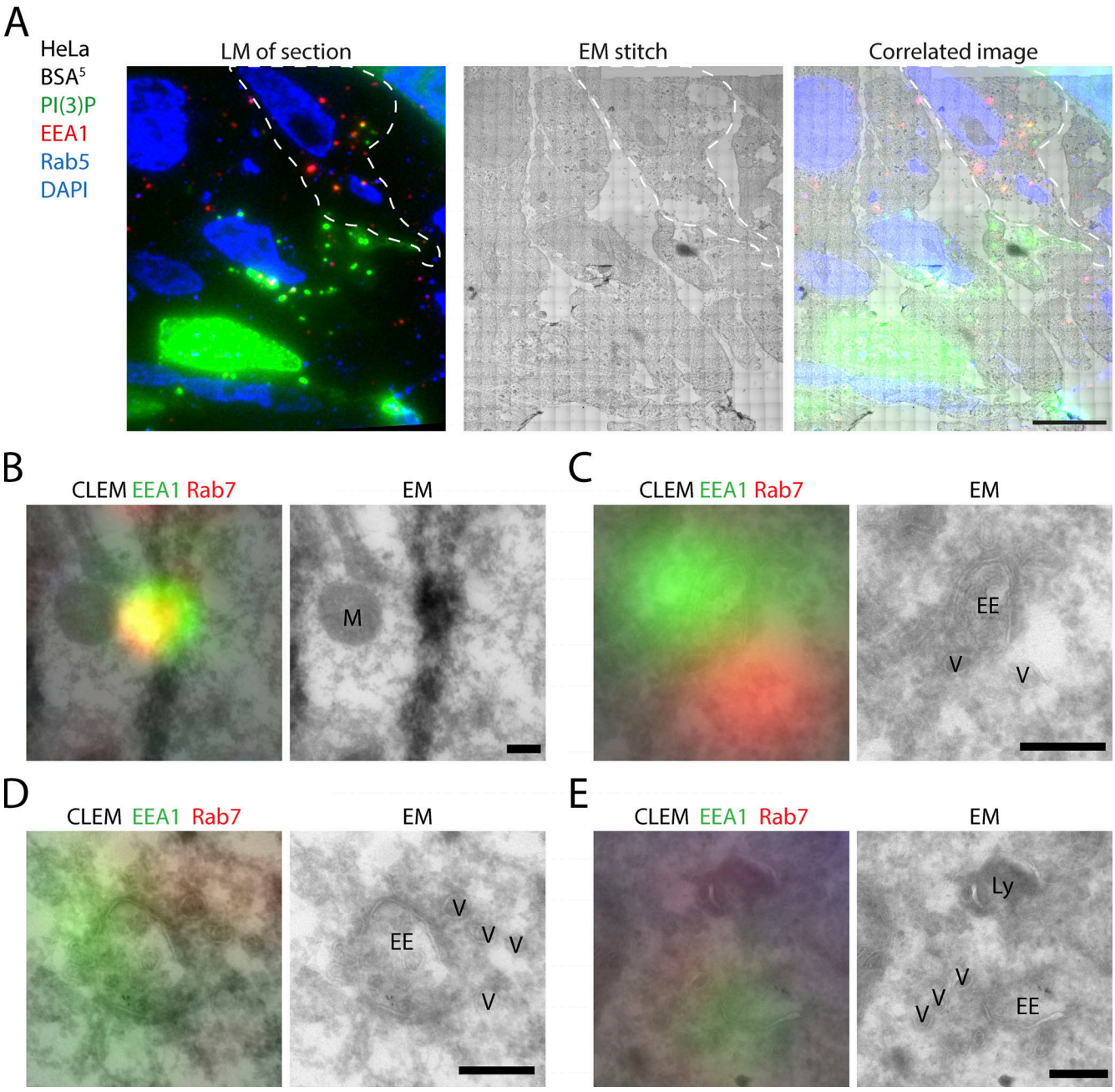

Figure S6. **CLEM of PI(3)P and Rab7/EEA1 colocalization. (A)** On-section CLEM of HeLa cells transfected with 2xFYVE-EGFP (PI(3)P) and immunolabeled for EEA1 and Rab5 with Alexa Fluor 568 and 647 secondary antibodies, respectively. Samples were prepared as described in Fig. 3. 2xFYVE-EGFP (PI(3)P) shows variable expression levels; only cells with low levels were selected (dashed outline) for analysis. **(B–E)** CLEM of EEA1 and Rab7 as described in Fig. 5, E and G. **(B)** Example of false-positive EEA1/Rab7 colocalization (solid arrowhead in Fig. 5 E) caused by fold (black mass) in the section. **(C)** CLEM of adjacent Rab7 and EEA1 signal (Fig. 5 E, open arrowhead). EEA1 marks an early endosomal vacuole, whereas Rab7 overlaps with adjacent tubulo-vesicles. **(D and E)** CLEM examples of occasional Rab7 and EEA1 colocalizations showing EEA1-positive early endosomes with Rab7-positive associated vesicles. EE, early endosome; Ly, lysosome; LM, light microscopy; M, mitochondrion; V, vesicle. Scale bars, 10 µm in overview; 200 nm in EM panels.

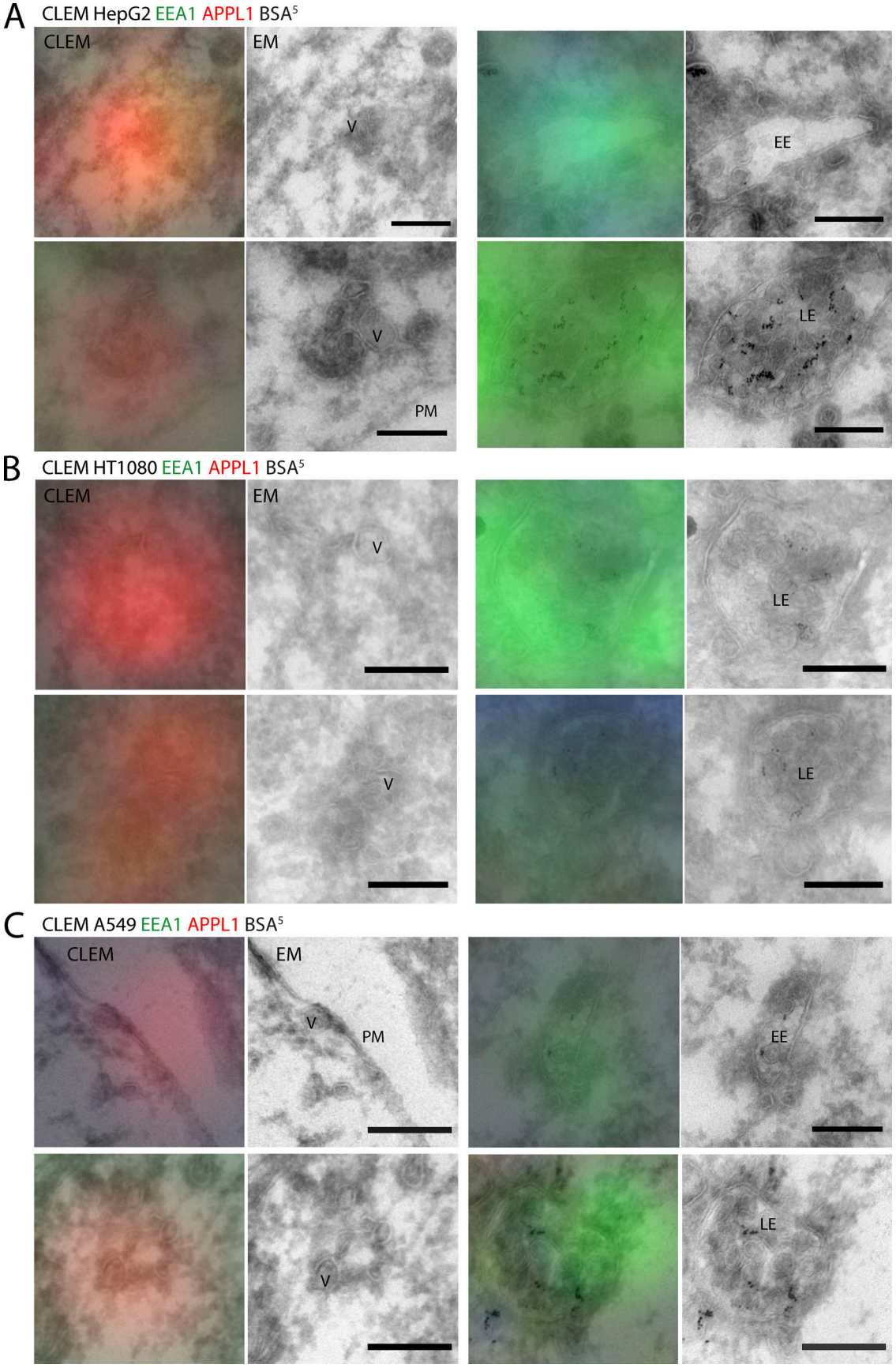

Figure S7. **Original CLEM and EM images from pseudocolored examples in Fig. 6. (A–C)** CLEM and EM images of pseudocolored images in main Fig. 6, A–C, respectively. EE, early endosome; LE, late endosomes; PM, plasma membrane; V, vesicle. Scale bars, 200 nm.

Provided online is one table. Table S1 lists organelle, colocalization, and SD values for Fig. 1.